remote sensing

MDPI

Article

Effect of Baseline Definition on Post-Fire Resilience Metrics Derived from Landsat Time Series in *Pinus halepensis*

Pedro Martín-Ortiz [1,2,*], Cristian Iranzo [1,2], Daniel Borini Alves [3], Raquel Montorio [1,2] and Fernando Pérez-Cabello [1,2]

[1] Department of Geography and Land Management, University of Zaragoza, Pedro Cerbuna 12, 50009 Zaragoza, Spain; c.iranzo@unizar.es (C.I.); montorio@unizar.es (R.M.); fcabello@unizar.es (F.P.-C.)
[2] University Institute of Research in Environmental Sciences (IUCA), University of Zaragoza, 50009 Zaragoza, Spain
[3] Programa de Pós-Graduação em Geografia, Universidade Estadual Vale do Acaraú, Avenida John Sanford, 1845, Sobral 62030-000, Ceará, Brazil; danielborini.geo@gmail.com
* Correspondence: pedro.martin@unizar.es; Tel.: +34-651365776

Highlights

- GEOBIA-based segmentation delineates homogeneous ecological units, reducing uncertainty in baseline selection for post-fire resilience assessment.
- NDVI time series combined with the spectral probability of belonging to *Pinus halepensis* allows distinguishing early greenness recovery from actual pine canopy recovery.
- NDVI alone may overestimate resilience in early post-fire stages, as shrub species dominate before the pine canopy fully recovers.

What are the main findings?

- NDVI in *Pinus halepensis* communities recovers within approximately seven years after wildfire, whereas structural pine canopy recovery requires more than 15 years.
- NDVI alone overestimates resilience, as early recovery stages are dominated by shrub species such as *Quercus coccifera*.

What are the implications of the main findings?

- Baseline selection critically influences the accuracy of remote sensing-based post-fire recovery assessments.
- Remote sensing assessments based solely on NDVI may misinterpret forest resilience in Mediterranean pine ecosystems.

Abstract

Wildfires have historically shaped Mediterranean ecosystems, fostering the adaptation of fire-resilient species such as *Pinus halepensis* Mill. Assessing post-fire resilience is essential to understand landscape recovery and guide forest management. This requires evaluating the speed, intensity, and trajectory of vegetation recovery relative to a defined baseline, although the influence of control point selection and baseline configuration remains unclear, despite its critical role in shaping the interpretation of recovery dynamics. This study proposes a methodological framework to assess the resilience of *P. halepensis* using 14-year Landsat time series following wildfire events, combined with image segmentation algorithms and Object-Based Image Analysis (GEOBIA). The analysis integrates two complementary vectors: (i) temporal evolution of NDVI and (ii) spectral probability of assignment to *P. halepensis*. Results indicate that NDVI suggests an average vegetation recovery time of seven years; however, spectral probability remains below 40% during this period, indicating slower tree cover recovery. Field inventories confirm that full recovery

Academic Editor: Víctor Fernández-García

Received: 10 March 2026
Revised: 21 April 2026
Accepted: 24 April 2026
Published: 28 April 2026

requires more than 15 years, with early stages dominated by shrublands, mainly *Quercus coccifera*. These findings show that NDVI alone overestimates resilience and that control selection and baseline configuration strongly influence assessments. GEOBIA enhances the ecological precision of resilience evaluation.

Keywords: remote sensing; wildfire; resilience; *Pinus halepensis*; baseline; Ecological Units (EU); GEOBIA

1. Introduction

For hundreds of thousands of years, wildfires have been a key natural factor in shaping the landscape of Mediterranean ecosystems [1,2]. However, socioeconomic transformations in recent decades, changes in land use [3], and trends in weather patterns [4,5] have increased the frequency and intensity of fires [6,7], altering natural fire regimes and compromising forest recovery and ecosystem services [8,9].

The most immediate consequence of fire is the destruction of vegetation, which has the most far-reaching ecological and landscape impact [10]. However, many species have developed adaptive strategies, including physio-morphological traits and reproductive mechanisms that allow them to resist or recover from fire disturbances [11,12]. The most prominent of these strategies in Mediterranean ecosystems include resprouting from dormant tissues that survive fire (resprouters), seed germination (obligate seeders) or the combination of both mechanisms (facultative) [13–16].

Pinus halepensis Mill. is a fire-adapted species [17]. Individuals of *P. halepensis* can store seeds in closed cones within the canopy for more than one reproductive cycle [18,19]. Seeds in these serotinous cones are protected from fire and are massively released after disturbance, finding optimal conditions for germination, seedling establishment, and growth [20,21]. However, many studies have pointed out that the current dynamics of very high-severity fires occurring within short time intervals may compromise the recovery of these species [22,23].

Satellite remote sensing has been widely used to monitor forest change at multiple scales [24–26]. The Landsat program (NASA-USGS), initiated in the early 1970s, is one of the most widely used due to its long-term data record. Since the 1980s, improvements in sensor technology have provided consistent multispectral imagery with 30 m spatial resolution and a 16-day revisit time [27–29]. In the long term, the use of multispectral time series (TS) allows a more detailed understanding of forest dynamics, facilitating the detection of patterns, trends, and seasonal variations in vegetation [30–32].

Vegetation regeneration can be assessed through spectral indices, which are simple indicators of fire impact [33]. The Normalized Difference Vegetation Index (NDVI) is one of the most widely used indicators of the rate of ecosystem recovery after a fire [34,35]. The suitability of NDVI stems from its general responsiveness to the amount of photosynthetic activity [36] and from its ability to monitor changes in vegetation cover across time series of images [37]. However, other spectral indices that combine multiple bands of the electromagnetic spectrum have also been used in the literature (e.g., Normalized Burn Ratio, NBR; Normalized Difference Moisture Index, NDMI; and Soil-Adjusted Vegetation Index, SAVI [38,39]).

Many studies have found a relationship between post-fire ecological recovery and greenness recovery levels as measured by spectral indices [27,40]. However, from an ecological and functional point of view, it remains unclear under what circumstances spectral recovery is assimilable to integral recovery of plant formations [41]. In this context, Bartels

et al. [42] point out that the term "recovery" is not clearly defined and that a connection must be established between spectral indicators and the ecological understanding of vegetation recovery.

Although resilience cannot be adequately analyzed with a single indicator, the characteristics that make some systems more resilient than others can be assessed by examining the rate, degree, and manner in which vegetation attributes are restored [43–45]. In recent years, ecosystem resilience has been linked to two separate concepts: "resistance" and "recovery" [46,47]. The concept of "resistance" reflects the ability of ecosystems to withstand disturbances [45,48]. "Recovery" refers to endogenous processes that return the disturbed system to a state of equilibrium. It considers the time that has passed between the disturbance and the achievement of a new stability, even though this new state does not coincide with pre-fire conditions [46].

Many studies use remotely sensed data, especially time series of spectral indices, to estimate post-fire forest resilience [49,50]. Most of these metrics are compared to a baseline, which functions as a reference measure to assess the post-fire ecosystem changes in relative terms [51,52]. Identifying baselines is a crucial phase in any discipline that uses the polysemous concept of resilience. The importance and complexity of using remotely sensed data is even greater due to the variability of the data and the difficulty of defining consistent references in a changing environment [53,54].

The literature distinguishes two different approaches for obtaining reference data and constructing the baseline. On the one hand, there is the approach in which the reference is based on pre-fire conditions analyzed in the same location where the fire occurred [55–57]. On the other hand, the reference is taken from control areas representative of the burned zone but not located in the same space where the fire occurred [58–60].

In a theoretical experimental framework for comparing burned and control areas, it is assumed that the burned zone would have exhibited the same structure and function as the control one if the fire had not occurred [61]. To properly select control areas, it is essential to have appropriate techniques and tools to identify homogeneous pre-fire zones [62]. Several authors have demonstrated similarity between burned and control areas using forest maps and high spatial resolution images [59], whereas others argue for pre-fire functional similarity based on biological parameters [62]. However, few studies explicitly ensure the similarity between burned and control areas [62] or evaluate the influence of different methods to define baselines, despite some research showing significant differences depending on the approach used [26]. To our knowledge, no consolidated method currently exists to assess the resilience of post-fire forest communities using vegetation index time series that considers the quality of the results according to the reference used [60].

Classification algorithms based on object recognition (e.g., landscape objects or patches) are particularly well-suited for multiscale analysis, providing greater accuracy and representativeness. These techniques focus on dividing images into relatively homogeneous objects that are distinct from their neighbors and have their own meaning. They allow us to obtain the objects' characteristics from spatial, spectral, and temporal perspectives [63]. Object-oriented classification techniques help us to define homogeneous pre-fire landscape units. From these units, we can derive control zones that are representative of burned areas.

The present study aims to analyze the resilience of forest communities dominated by *P. halepensis* affected by fires in northeastern Spain using time series of multispectral images. To this end, the burned area is segmented into homogeneous ecological units by object-oriented classification (Geographic Object-Based Image Analysis—GEOBIA) at pre-fire time. Then, the influence of different criteria on the baseline design and its impact on resilience estimates is evaluated. Two complementary analysis vectors are used: (i) the temporal evolution of vegetation indices, evaluated using statistical analysis and relative

difference calculations; and (ii) the spectral probability of assignment to *P. halepensis*. This work constitutes a methodological proposal specifically designed to evaluate the resilience of fire-affected forest communities.

Based on this approach, the following working hypotheses are proposed: (i) inconsistency in the selection of control areas compromises the construction of baselines and, consequently, may lead to incorrect analyses of resilience; (ii) the exclusive use of vegetation indices is not sufficient to obtain conclusive results on community resilience; (iii) *P. halepensis* pine forests do not always have a high ability to recover after a fire.

2. Materials and Methods

The methodological workflow followed in this study (Figure 1) begins with the selection of wildfire events, for which a harmonized Landsat time series was constructed. Spectral indices, including NDVI, were derived as the main variables for analysis. In parallel, GEOBIA-based segmentation was applied to delineate ecological units on which the recovery analysis was conducted. Vegetation mapping integrated spectral, topographic, and lithological variables, enabling the characterization of vegetation types and the estimation of the temporal probability of *P. halepensis*. Different pixel sampling strategies and baseline definitions were implemented to quantify post-fire resilience through alternative approaches. Finally, results were validated against field-based vegetation inventories.

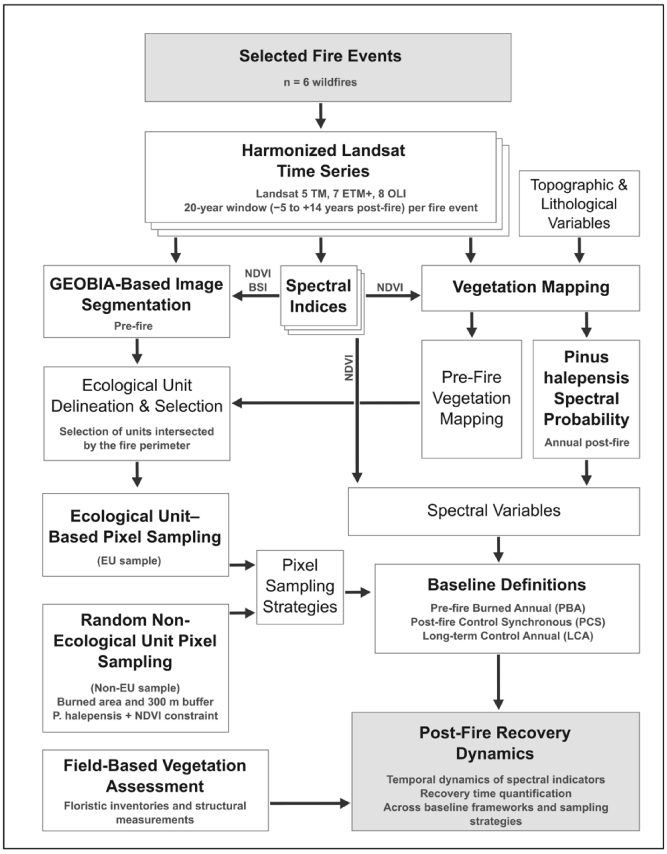

Figure 1. Methodological workflow of the study.

2.1. Study Area

Six forest fires affecting *P. halepensis* stands in Aragón, northeastern Spain, were selected and distributed across different areas of the region's forest territory. These fires formed a transect that allowed us to capture, as far as possible, the climatic and topographic

variability of the Mediterranean landscapes in which this tree community develops (see Table A1 in Appendix A).

As shown in Figure 2A, the analyzed fires (whose names refer to the place closest to the burned area) are primarily located in the Ebro Depression, the foothills of the Iberian System, and the Pyrenees. These fires correspond to *Riglos* (2001), *Zuera* (1995), *Talamantes* (1991), *Tabuenca* (1994), *Fuentes* (1987), and *Jaulín* (2009). The burned areas range from 400 to 3000 hectares. The largest are *Riglos* and *Zuera*, and the smallest are *Jaulín* and *Fuentes*. According to Köppen's climate classification [64], the analyzed areas are included in the BSk (*Cold semi-arid climate*) or Cfa (*Humid subtropical climate*) types. The average annual temperature ranges from 11 °C to 16 °C, and the average annual rainfall ranges from 400 to 650 mm. Most of the rainfall occurs in the spring and autumn months. However, the altitude and orientation of the different sectors generate significant microclimatic variability along the transect formed by the fires.

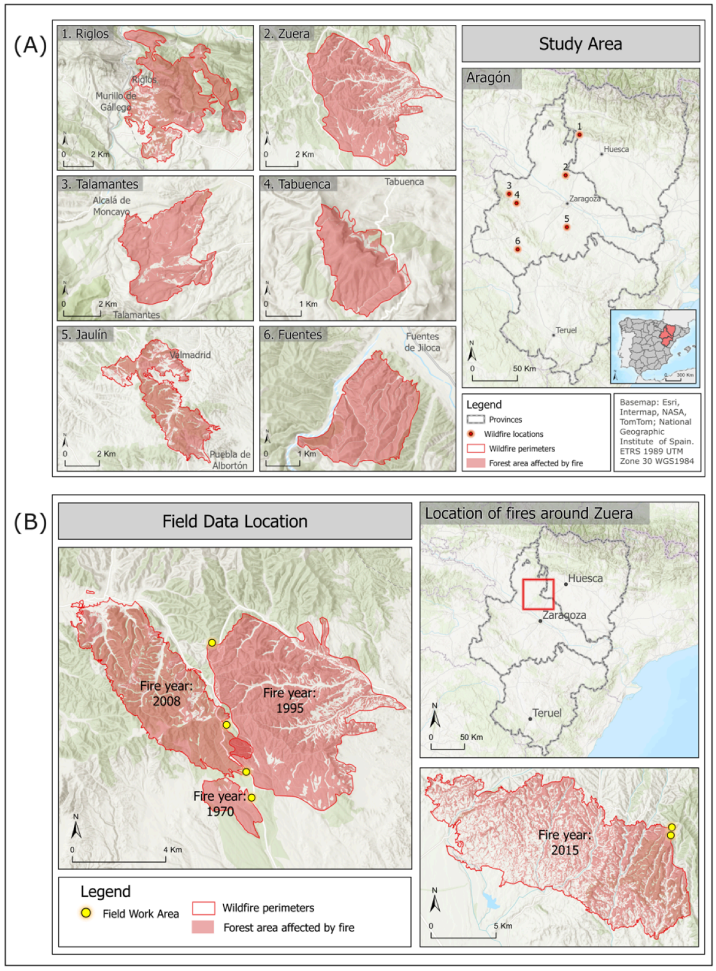

Figure 2. Study area. (**A**) Fires analyzed in the study. (**B**) Fieldwork locations near *Zuera,* including a northern fire (2015) near *Luna*, displayed separately for clarity; Yellow points indicate the location of the floristic inventories. The place names (*Zuera*, *Luna*, *Riglos*, *Talamantes*, *Tabuenca*, *Jaulín*, and *Fuentes*) correspond to municipalities in Aragón, Spain.

We delineated the burned areas using the fire database from the Government of Aragón and the spectral indices Normalized Burn Ratio (dNBR) [65] and Relative Delta Normalized Burn Ratio (RdNBR) [66] applying the threshold values proposed to delineate burned areas by Key and Benson (2006), within the framework of the FIREMON (Fire Effects Monitoring and Inventory Protocol) project [65], and by Miller and Thode (2007), respectively [66].

2.2. Processing of a Multitemporal Image Time Series

This study used a harmonized series of Landsat images, following the methodology proposed by Alves et al. [67] which covers a 20-year period for each fire (5 years before and 14 years after, add the year of the fire).

The present study used calibrated top-of-atmosphere (TOA) reflectance data sets corresponding to Landsat Collection 2—Tier 1 Level 1. These were acquired by the Landsat 5 TM (Thematic Mapper), Landsat 7 ETM+ (Enhanced Thematic Mapper Plus), and Landsat 8 OLI (Operational Land Imager) sensors. Clouds and cloud shadows were identified and masked using the Landsat pixel quality assessment (QA) band available in Google Earth Engine (GEE), and images with insufficient valid observations were excluded from the analysis. Data from the three Landsat sensors were harmonized and merged into a single time series through bandpass adjustment (using Landsat 8 as reference) and normalization to ensure cross-sensor consistency.

The collections underwent a harmonization process that included radiometric, atmospheric, topographic, and BRDF (Bidirectional Reflectance Distribution Function) corrections, by adapting open codes implemented in the Jupyter Notebook (v7.5.5) [68] and GEE [69] environments (Figure 3). In addition, spectral indices were calculated and gap-filling techniques were applied to maximize the availability of observations free of clouds and other disturbances.

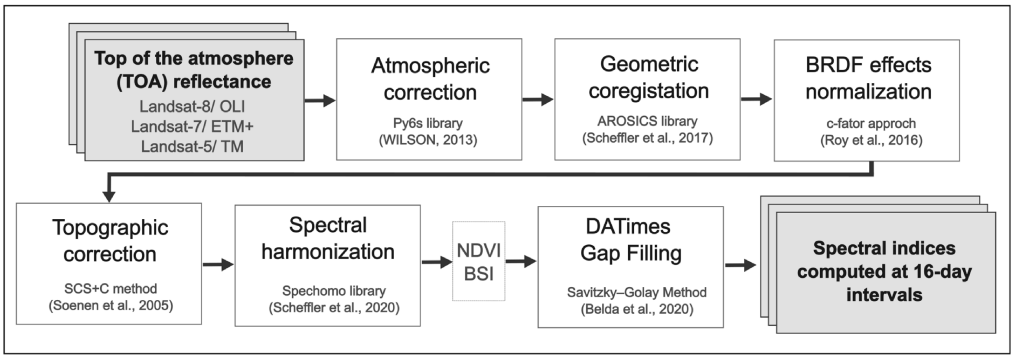

Figure 3. Methodological flowchart for the construction of the time series. References for this figure: Wilson et al. [70], Scheffler et al. [71], Roy et al. [72], Soenen et al. [73], Scheffler et al. [74], and Belda et al. [75].

Atmospheric correction: TOA images were atmospherically corrected using a standard algorithm based on the 6S radiative transfer model via the Py6s Python API [70], with scripts adapted from Nguyen et al. [76] and Murphy [77], yielding surface reflectance (BOA) for each dataset.

Geometric correction: Spatial automatic registration was implemented using the Automated and Robust Open-Source Image Co-Registration Software (AROSICS, v1.13.0) Python API [71], following the official API documentation (https://danschef.git-pages.gfz-potsdam.de/arosics/doc/index.html; accessed on 9 March 2026). The co-registration process was performed by phase correlation to estimate sub-pixel displacements. The cloud-free Landsat record with the lowest geometric mean square error, according to the data producer, was used as a reference.

Normalization of the bidirectional reflectance distribution function (BRDF): BRDF effects were calculated and corrected using the general method developed by Roy et al. [72] for Landsat data, based on the c-factor approach. The correction was performed by applying calibrated and validated coefficients per band, adjusting the viewing angle of the images to obtain nadir-adjusted BOA data. BRDF normalization was implemented on the GEE platform, using open source scripts from Nguyen et al. [76].

Topographic correction: To minimize the impact of topographic morphology on the spectral signal, topographic correction was applied using the SCS + C method (Sun-Canopy-Sensor with Semiempirical Moderator) [73]. This procedure was coded from the open scripts of Nguyen et al. [76] and Poortinga et al. [78] in GEE. The Copernicus Global Digital Elevation Model (DEM) at 30 m [79] was used to obtain the necessary elevation and slope parameters.

Bandpass adjustment: The spectral harmonization was processed using the Python SpecHomo library [74], using Landsat 8 (OLI) as reference and linear regressions with 50 clusters (https://github.com/GFZ/spechomo; accessed on 9 March 2026). The time series of images was used to calculate the NDVI spectral indices (Equation (1)) [80] and Bare Soil Index (BSI) (Equation (2)) [81]. Finally, gap filling in the time series was carried out using the DATimes software (v1.13) [75]. The Whittaker smoother [82] was applied (lambda = 1000) to interpolate missing data, followed by the Savitzky–Golay spatiotemporal smoothing technique [83]. The Savitzky–Golay filter was implemented with a window span of 7 satellite acquisitions and a polynomial degree of 2. Image allocation was carried out at Landsat's inherent 16-day orbital intervals. However, in this study we refer to biweekly periods, as this approximation facilitates temporal aggregation and interpretation without significant loss of accuracy compared to the actual 16-day interval.

$$\mathrm{NDVI} = \frac{\mathrm{NIR} - \mathrm{RED}}{\mathrm{NIR} + \mathrm{RED}} \quad (1)$$

$$\mathrm{BSI} = \frac{(\mathrm{RED} + \mathrm{SWIR}) - (\mathrm{NIR} + \mathrm{BLUE})}{(\mathrm{RED} + \mathrm{SWIR}) + (\mathrm{NIR} + \mathrm{BLUE})} \quad (2)$$

2.3. Vegetation Mapping

Cartographic products derived from the digital classification of Landsat multispec-tral imagery were used to evaluate the spatial distribution of pre-fire vegetation and to estimate the annual spectral probability of assignment to *P. halepensis* within the analyzed time interval (pre- and post-fire), following the method proposed by Iranzo et al. [84]. Annual vegetation maps were produced, with predictors like NDVI and spectral bands calculated each year to capture interannual variability.

Supervised classification was implemented in Python using scikit-learn [85] and imbalanced-learn [86], with 1323 training points covering seven forest types, six shrubland types, and one bare ground category (see Table A2 in Appendix B), supported by national forest and land cover datasets. Specifically, these labels were derived from expert visual interpretation of national forest maps and orthophotos, with 770 forest and 533 shrub labels. The data were split into training and validation subsets (70/30) using stratified sampling. Predictor variables included Landsat spectral bands (blue, green, red, near-infrared-NIR and shortwave infrared-SWIR1 and SWIR2), NDVI, altitude, relief shading, and lithology (see Table A3 in Appendix C), combined with data augmentation (SMOTE [87], ADASYN [88]), subsampling (Tomek Links [89], Random Undersampling [86]), and two machine learning algorithms: Random Forest (RF) [90] and Support Vector Machines (SVM) [91]. All combinations of augmentation and subsampling techniques were systematically evaluated using cross-validation, and the final configuration was selected based on the best overall accuracy and kappa performance. Among the wide range of machine learning algorithms applied to land cover and vegetation species classification in remote sensing, SVM and RF have consistently demonstrated superior overall performance [92].

Hyperparameters for both models were optimized using grid search with two-fold stratified cross-validation [93]. For the SVM model, the evaluated hyperparameters included regularization parameter values (C = 5, 15, 25), kernel types (radial basis function

and sigmoid), and gamma settings (scale and auto, defined as 1 divided by the number of features). The final SVM model was trained using C = 25, gamma = auto, and the radial basis function kernel. For the RF model, the grid search evaluated the number of estimators (500 and 600), minimum samples per leaf (5, 10, 15, 20), and minimum impurity decrease (0.0, 0.05, 0.1), with the optimal configuration consisting of 500 trees, a minimum of 5 samples per leaf, and a minimum impurity decrease of 0.0.

Therefore, these two models were selected for this study. Model performance was evaluated with overall accuracy (OA) and the kappa index, prioritizing underrepresented classes. The SVM model using Tomek Links subsampling achieved the highest performance (OA = 0.92; kappa = 0.88), whereas the RF model showed slightly lower overall performance (OA = 0.89; kappa = 0.86), with more concentrated misclassification patterns that negatively affected overall accuracy. Consequently, the SVM model was selected to generate thematic maps of forest distribution across the study period.

2.4. Image Segmentation and Object-Based Classification

To identify the spatial distribution of landscape units or patches, we applied an adapted version of the algorithm proposed by Tassi and Vizzari [94], which integrates object-oriented classification methodologies (GEOBIA) with Machine Learning algorithms in GEE. This approach enabled the delineation of homogeneous units in both burned areas and a 300 m control strip adjacent to the fire perimeter.

All available images and spectral indices (NDVI and BSI) (see Table A3 in Appendix C) corresponding to the three years prior to each fire were selected from the harmonized image time series. These data were used to generate a set of variables (outBands), which integrated the median of the visible (VIS), near-infrared (NIR), and shortwave infrared (SWIR) spectral bands. This set also included descriptive statistics of the spectral indices, such as minimum, maximum, mean, median, and standard deviation. A random sample of high-probability pixels was created for pre-fire vegetation classification and used for training. Both outBands and sample points were uploaded to the GEE, where the GEOBIA algorithm was applied.

This algorithm is structured in different phases, with the first phase being the image clustering or segmentation stage using the Simple Non-Iterative Clustering (SNIC) method, developed by Crowley et al. [95]. This method groups homogeneous pixels by combining spectral and spatial data, accounting for local variability with normalization factors (S and M). Key parameters included compactness (set to 0 for circular segments), connectivity (8 for diagonal neighbors), seed shape (initial points spaced 20 pixels apart), and inter-seed distance (256 pixels) to control segment size and distribution.

Each pixel was assigned to the nearest segment seed based on combined spectral (five bands) and spatial (x, y coordinates) affinity. The SNIC algorithm (Equation (3)) [96] combines spectral distance ($\|c_i - c_j\|$) and spatial distance ($\|x_i - x_j\|$) using normalization factors s and m, where $s = \sqrt{(N/K)}$ (N = total pixels, K = expected segments). Here, N is fixed by the image size, while m (compaction coefficient) and s (number of seeds) control the size and shape of the segments.

$$d_{j,k} = \sqrt{\frac{||x_j - x_k||_2^2}{s} + \frac{||c_j - c_k||_2^2}{m}} \quad (3)$$

The second phase of the process corresponds to the textural characterization of the segmented objects using the Gray-Level Co-occurrence Matrix (GLCM). The result was the segmentation of the landscape into homogeneous units, or patches. In the framework of this research, these patches will be interpreted as functional ecological units (EU).

2.5. Baseline Establishment

Three different baselines were created by combining spatial and temporal criteria (Figure 4).

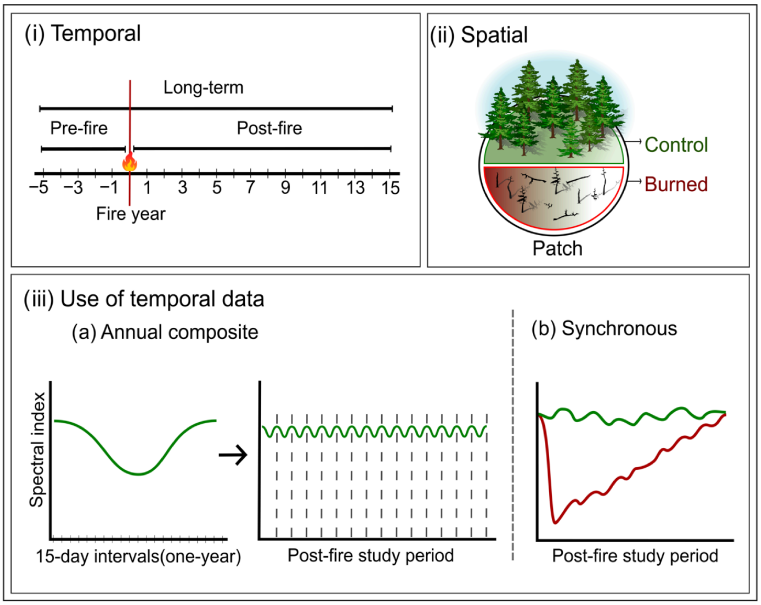

Figure 4. Criteria for baseline construction using different approaches, showing spatial and temporal methods, including annual composites and synchronous tracking.

- Pre-fire Burned Annual composite (PBA): This baseline uses the burned area as its own reference prior to the fire. The comparison is based on an annual NDVI composite integrating data from the five years before the fire.
- Post-fire Control Synchronous (PCS): This baseline relies on unburned control areas (i.e., areas that remained unaffected by fire throughout the entire study period) within a 300 m buffer surrounding the fire perimeter. NDVI trajectories of the burned and control areas are compared synchronously (i.e., date by date) over the 15 years following the fire.
- Long-term Control Annual composite (LCA): This baseline also relies on unburned control areas but integrates both pre- and post-fire periods. The annual composite combines five pre-fire years and 15 post-fire years, producing a long-term reference curve that captures the typical vegetation phenological pattern.

Additional considerations apply to the PBA and LCA composites: (i) annual composites are constructed using the median NDVI values for each 15-day interval, ensuring that the baseline reflects the typical phenological behavior of vegetation; (ii) a five-year pre-fire window was selected to minimize interannual variability and particularly to reduce the influence of extreme climatic anomalies that often precede fire events.

2.6. Comparison Between Baselines and Temporal Evolution of NDVI in Burned Areas

2.6.1. Pixel Sampling

Two different pixel sampling strategies were implemented in this study:

(1) GEOBIA-adjusted patch sampling (EU sample): Patches or EUs delineated prior to the fire using the GEOBIA algorithm were selected. These patches were intersected by the fire perimeter, splitting each unit into burned and non-burned (control) sectors with comparable surface areas. For each patch, 70 pixels were randomly sampled from the burned sector and 70 from the control one. Sampling covered all biweekly periods from five years before the fire to 14 years after the event.

(2) Random sampling not adjusted to patches (non-EU sample): For each fire, 70 pixels were randomly extracted from the burned area and from an external control zone defined by a 300 m buffer around the affected area, chosen as a nearby distance that maintains environmental conditions comparable to the burned area. Sampling in this control area was restricted to areas classified as *P. halepensis* according to the Forestry Map of Spain and with NDVI values higher than 0.2. Non-EU samples represent a standard, unsegmented random sampling approach commonly used in studies of this type, intentionally not conditioned by GEOBIA delineation. To ensure the same number of observations in both pixel sampling strategies, a number of samples equivalent to the number of patches used in the analysis was generated.

2.6.2. Statistical Analysis

First, the similarity between burned and control areas within the same patch was assessed using patch-adjusted pixel samples from the five years before the fire (R^2, bias, MAE, RMSE). These metrics were computed directly from paired burned and control pixel observations within the same unit, based on a statistical comparison of their agreement.

Next, the baselines generated using the three different approaches were compared with post-fire NDVI using inferential statistics (ANOVA or Kruskal–Wallis). Comparisons were done biweekly, analyzing pixels adjusted and not adjusted to patch boundaries separately. In PCS, burned-area NDVI was compared directly with the control area using 70 pixels per interval. In PBA and LCA, a baseline was built for each pixel (70 per interval) using the median NDVI of the same biweekly period across years. PBA used five years before the fire; LCA used five years before and 14 years after. Around 20,500 comparisons were performed to study NDVI over time.

These analyses allowed estimation of recovery times in years for each burned area, and inferential statistics were used to check for significant differences between results.

2.6.3. Calculation of Relative Differences

To establish direct comparisons between baselines and burned area, relative differences (RD) were calculated for each fortnight (Equation (4)). To this end, the median (Me) NDVI of the 70 pixels sampled each fortnight was obtained in both the burned area and the respective baseline. This generated a single, representative value per fortnight for each line. The relative difference formula was applied to these values. Those close to 0% indicated no change, while positive or negative values reflected increases or decreases in vegetation compared to the baseline.

$$\mathrm{RD}(\%) = \left(\frac{\mathrm{Me\ NDVI_{Burned}} - \mathrm{Me\ NDVI_{Baseline}}}{\mathrm{Me\ NDVI_{Baseline}}} \right) * 100 \quad (4)$$

2.6.4. SAM

The Spectral Angle Mapper (SAM) method [97] was used to evaluate intra-annual similarity between phenological profiles of the burned area and different baselines. Originally developed for hyperspectral mineral analysis [98], SAM has been adapted for spectro-temporal data by calculating the angle between NDVI time series vectors [99,100]. The SAM method calculates the angle between two vectors in n-dimensional space. Smaller angles indicate higher similarity between annual NDVI trajectories. The spectral angle θ (in radians) between the burned area and baseline NDVI vectors was computed as described in Equation (5), with n observations over time i.

$$\theta = cos^{-1} \left(\frac{\sum_{i=1}^{n} \mathrm{NDVI_{Burned}} \cdot \mathrm{NDVI_{Baseline}}}{\sqrt{\sum_{i}^{n} \mathrm{NDVI^2_{Burned}}} \cdot \sqrt{\sum_{i}^{n} \mathrm{NDVI^2_{Baseline}}}} \right) \quad (5)$$

2.7. Field Data

During the spring of 2023, several field campaigns were carried out to collect information on vegetation composition and structure (specific diversity, cover, and height) in areas affected by fires in different years. The objective was to collect data on the timing of post-fire vegetation recovery for comparison with the results derived from the spectral analysis vectors. For this purpose, a chronosequence generated by the occurrence of several fires in the area surrounding the 1995 *Zuera* fire (1970, 1995, 2008, and 2015) was used (Figure 2B). All of these fires had similar characteristics and were representative of different stages of the post-fire recovery process. Floristic inventories were performed in burned and adjacent control areas, grouped into two chronosequences: ≤15 years and >15 years since fire. The Linear Transect Inventory Method (MIFC) [101] was applied in 10 × 2 m plots. A total of 1091 individuals were recorded across 18 inventories (controls, recent fires, and older fires). The analysis focused on *P. halepensis* and *Q. coccifera*, estimating crown area and height for each individual. Floristic inventories were conducted in burned areas and adjacent unburned control sites, grouped into two chronosequences: ≤15 years and >15 years since fire. The Linear Transect Inventory Method for Phanerophytes and Camephytes (MIFC) [101] was applied in plots measuring 10 m × 2 m. A total of 1091 individuals were recorded across 18 inventories, including control plots, recent burns, and older burns.

3. Results

3.1. Results of Object-Based Image Analysis

Using object-oriented classification (GEOBIA), 370 ecological units (EUs) were identified in burned areas and adjacent forest strips. Nineteen EUs dominated by *P. halepensis* that intersected the fire perimeter and had comparable proportions of burned and unburned areas were selected, covering approximately 780 hectares, of which 360 were within the burned area. Figure 5 shows a cartographic example of the Zuera fire with the selected EUs.

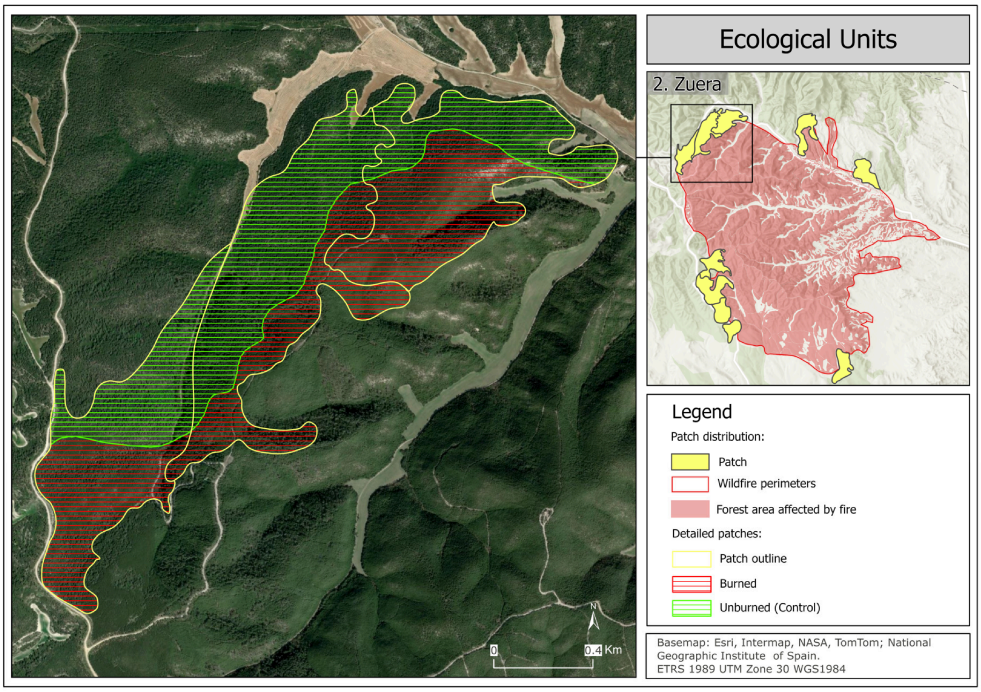

Figure 5. Pre-fire ecological units of the 1995 Zuera fire, showing three units with terrain-adapted boundaries and distinguishing burned (red) from control (green) areas.

Table 1 shows the similarity between burned and control sectors within each EU using pre-fire NDVI. Based on sampled data within each EU, the subsequently burned

and corresponding control sectors are compared using a set of validation statistics. High agreement was observed across all EUs, with R^2 values ranging from 0.816 to 0.990 and low MAE, RMSE, and bias values, indicating sector homogeneity and the absence of systematic deviations.

Table 1. Pre-fire similarity indices between burned and unburned sections within the same EU based on NDVI time series.

Fire	Pre-Fire Correspondence Levels Between Burned and Control Areas				
	ID [1]	R^2	Bias	MAE	RMSE
Riglos	1	0.816	0.019	0.043	0.055
	2	0.925	0.009	0.024	0.030
	3	0.934	−0.007	0.017	0.021
	4	0.962	−0.008	0.016	0.020
	5	0.941	−0.016	0.019	0.025
Zuera	1	0.989	0.022	0.022	0.024
	2	0.925	0.031	0.031	0.037
	3	0.975	0.003	0.008	0.011
	4	0.973	0.009	0.013	0.015
	5	0.990	0.007	0.008	0.009
	6	0.990	0.010	0.010	0.012
	7	0.985	0.001	0.006	0.008
	8	0.971	0.039	0.039	0.041
	9	0.987	0.001	0.006	0.008
	10	0.946	0.020	0.022	0.024
Talamantes	1	0.950	0.025	0.025	0.027
Tabuenca	1	0.912	−0.009	0.012	0.020
Jaulín	1	0.915	−0.017	0.018	0.021
Fuentes	1	0.891	−0.017	0.024	0.028

[1] ID: unique code identifying each ecological unit in the study, useful for reference and potential replication.

3.2. Phenological Pattern of P. halepensis

3.2.1. Comparison Between EU and Non-EU Samples

The development of annual NDVI composites for the baselines (PBA and LCA) allowed characterizing the apparent phenology (satellite-derived phenology, according to Younes et al. [102]) of *P. halepensis*. Figure 6 compares the estimated vegetative period from the NDVI samples of the EUs identified in the Zuera fire (selected for having the largest number of EUs) with that obtained from independent samples of 70 pixels randomly distributed (hereafter referred to as the non-EU sample). NDVI showed a seasonal phenological pattern, with a moderate decrease in summer and peaks in winter, reflecting the summer drought and higher photosynthetic activity during winter.

Clear differences were observed between the EUs (object-based sampling) and the non-EU (random sampling) sample. In general, the EUs exhibited higher NDVI values, remaining above 0.5 throughout the annual cycle, and showed narrower 95% confidence intervals, indicating greater internal homogeneity. In contrast, the non-EU samples, although corresponding to the same vegetation type and nearby areas, showed higher heterogeneity and greater dispersion in NDVI values.

These differences can be attributed to the fact that pixel samples within the EUs correspond to very homogeneous pine forest stands, both in composition and spectral behavior. In contrast, sampling pixels without considering functional EUs may include pine stands with varying levels of shrub presence; although most species show very similar

phenological behavior, the greater heterogeneity of these mixed stands generally results in slightly lower NDVI values.

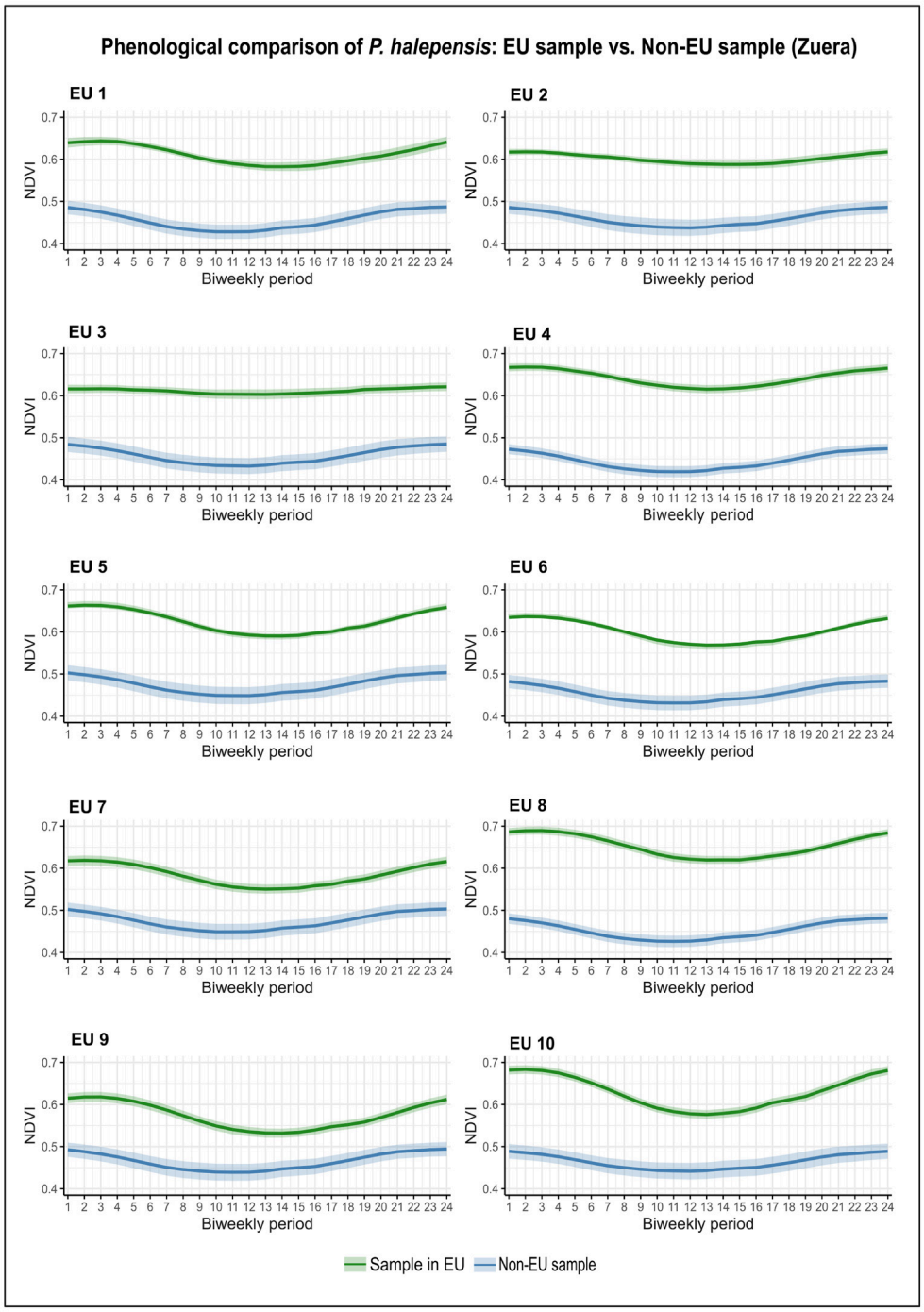

Figure 6. Comparison of the vegetative cycle of *P. halepensis* using EU (green) and non-EU (blue) samples for the *Zuera* fire. It shows the phenological pattern of each EU relative to a non-EU sample.

3.2.2. Intra-Annual Apparent Phenology of the EU: Comparison Between the Burned Sector and the Baselines

Over the 14 years following the fire, the SAM method assessed the phenological similarity between the burned areas and the baselines (Figure 7), serving as an indicator of photosynthetic recovery.

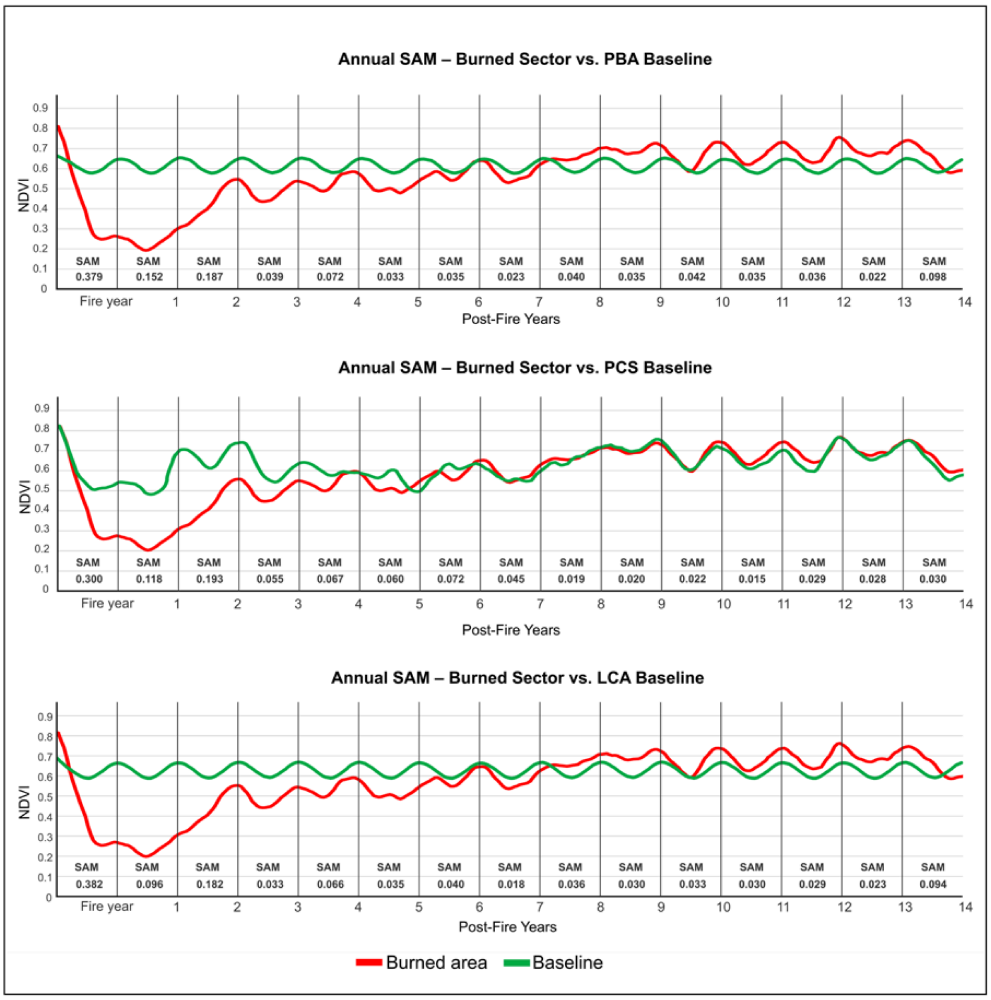

Figure 7. Temporal evolution of SAM values in a burned EU (*Zuera*). Progressive decrease in SAM values reflects phenological recovery post-fire (green line: baseline; red line: evolution of the burned area). Baselines: PBA (Pre-fire Burned Annual composite), PCS (Post-fire Control Synchronous), and LCA (Long-term Control Annual composite).

SAM values decreased progressively, reflecting a gradual phenological recovery. From the fifth post-fire year onward, values stabilized below 0.1 radians across all EUs and baselines, indicating high phenological similarity, although some EUs reached this stability earlier. Phenological stability persisted in the following years, with minor variations in some cases, as shown in Figure 8.

3.3. Identification of the Year of Convergence of Baselines and Burned Area

The differences between NDVI values in the burned areas and each baseline were evaluated for all available fortnights using relative differences (%) and inferential statistical analysis. The results allowed us to identify a relationship between the periods without statistically significant differences and the values of the relative difference. Based on this relationship, a threshold of ±3.5% was established to consider spectral recovery achieved, given that in 95% of the fortnights without significant differences the relative difference was equal to this threshold or closer to 0. Figure 9 shows the temporal evolution of the NDVI in the burned sector of an EU compared to its baseline (PCS), including the relative differences and the results of the inferential analysis. The recovery year for each EU was defined as the first year in which NDVI values remained above the −3% threshold for at least 12 consecutive months.

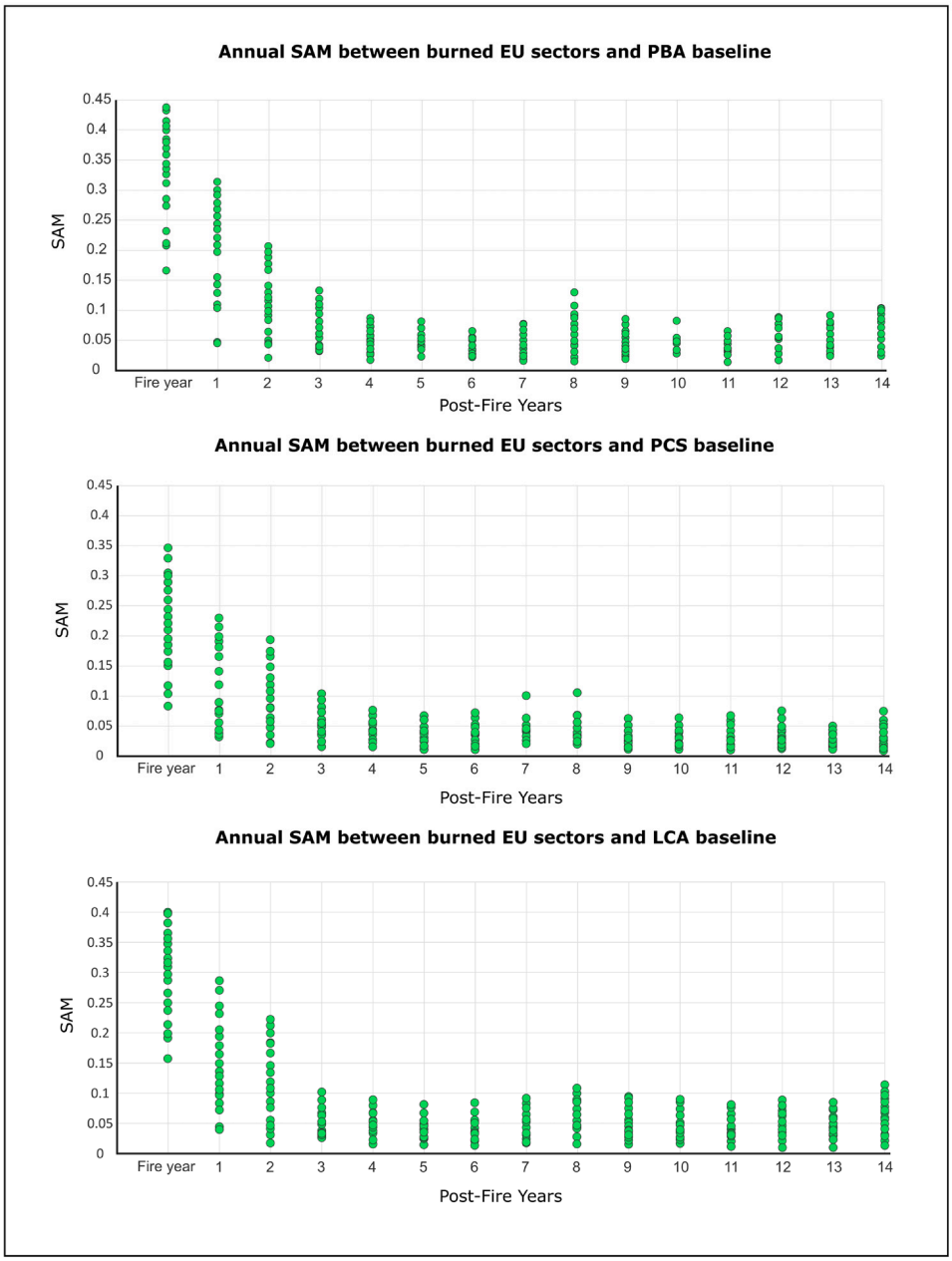

Figure 8. Temporal evolution of SAM values across all EUs. Each point represents the SAM value of each EU in that post-fire year. SAM values stabilized below 0.1 radians from the fifth post-fire year. SAM values stabilized below 0.1 radians from the fifth post-fire year. Baselines: PBA (Pre-fire Burned Annual composite), PCS (Post-fire Control Synchronous), and LCA (Long-term Control Annual composite).

The recovery year was determined using the constructed baselines and pixel samples (EU and non-EU). No statistically significant differences were found between the recovery times obtained with each baseline approach (p-value = 0.487), although small variations were observed depending on the baseline used.

The recovery times of the EUs (Table 2) showed considerable variability, ranging from 3 to 13 years post-fire, reflecting the heterogeneity of recovery processes among the different ecological units. The overall recovery period was concentrated around an average of approximately seven years. It should be noted that, according to any of the baselines used, three EUs (*Tabuenca*, *Jaulín*, and *Fuentes*) did not achieve recovery of the burned sector.

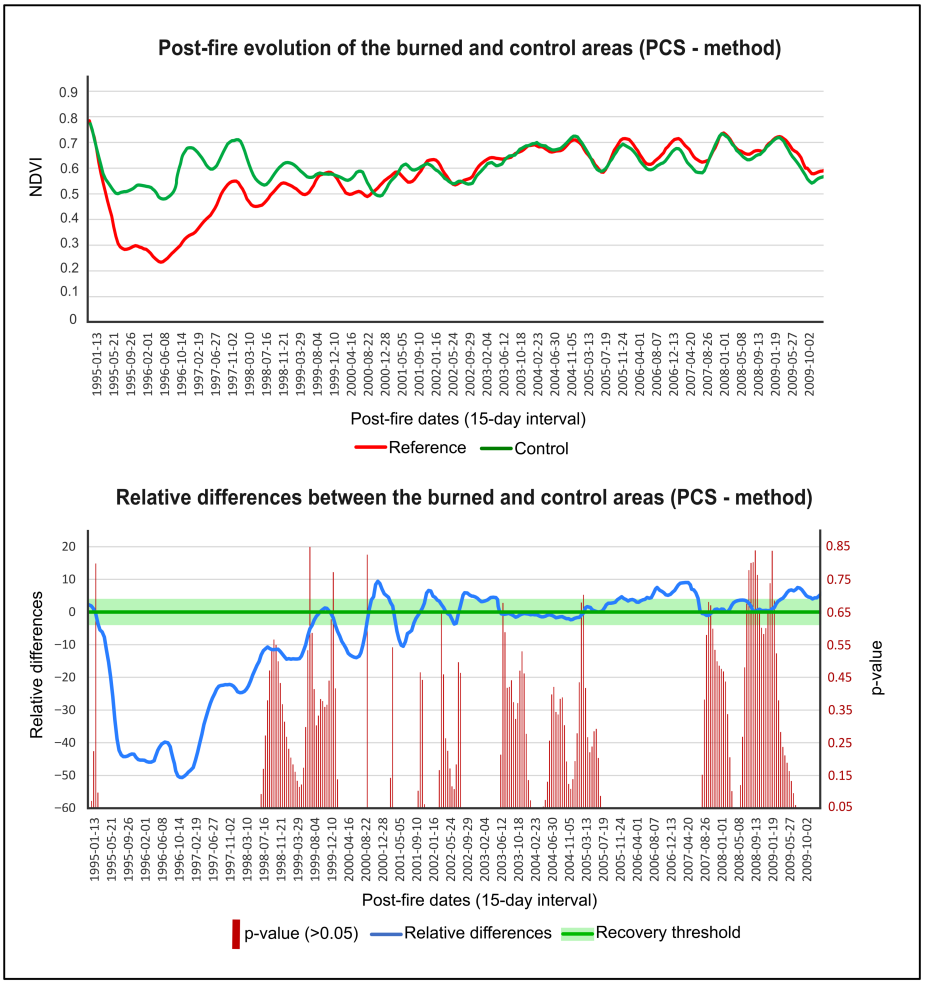

Figure 9. Biweekly NDVI evolution of a burned EU in Zuera (red) and its PCS baseline (green), showing relative differences (blue), statistical test *p*-values, and the recovery threshold (green).

Table 2. Levels of similarity between the burned and control sectors within the EUs.

Fire	Pre-Fire *P. h.* Prob (EU)	PBA		PCS		LCA		
		NDVI Time [1]	*P. h.* Prob [2]	NDVI Time [1]	*P. h.* Prob [2]	NDVI Time [1]	*P. h.* Prob [2]	*P. h.* Prob Recovery Time [3]
Riglos	80%	7	10%	12	10%	10	10%	-
	82%	7	30%	12	39%	12	39%	14
	79%	9	18%	9	18%	9	18%	-
	87%	12	37%	12	37%	12	37%	14
	85%	7	26%	10	27%	10	27%	13
Zuera	88%	4	40%	5	44%	5	44%	13
	84%	5	32%	5	37%	6	44%	8
	89%	3	28%	3	28%	5	43%	11
	83%	2	21%	3	22%	6	30%	12
	87%	8	25%	7	10%	8	25%	13
	80%	6	18%	8	40%	8	40%	11
	83%	6	27%	5	23%	6	27%	12
	85%	6	13%	5	9%	6	13%	12
	78%	6	8%	9	38%	9	38%	9
	82%	6	6%	9	14%	9	14%	13
Talamantes	85%	13	40%	10	10%	11	20%	13
Tabuenca	78%	-	-	-	-	-	-	-
Jaulín	79%	-	-	-	-	-	-	-
Fuentes	81%	-	-	-	-	-	-	-

[1] Years between the wildfire and NDVI recovery. [2] Probability of assignment to *P. halepensis* in the year of NDVI recovery. [3] Years between the wildfire and the equalization of assignment probability to *P. halepensis*.

Table 3 presents the estimated recovery times for the non-EU samples from each fire event. Considerably shorter recovery periods were observed for the non-EU samples than for the EU ones from the same fires, with values ranging from three to six years. However, as in the EU, the non-EU samples associated with the *Tabuenca*, *Jaulín* and *Fuentes* fires also failed to recover the burned sector.

Table 3. Recovery of NDVI and probability of belonging to *P. halepensis* for each fire when analyzing non-EU samples.

Fire	Pre-Fire *P. h.* Prob	PBA		PCS		LCA		
		NDVI Time [1]	*P. h.* Prob [2]	NDVI Time [1]	*P. h.* Prob [2]	NDVI Time [1]	*P. h.* Prob [2]	*P. h.* Prob Recovery Time [3]
Riglos	65%	4	20%	5	25%	4	20%	8
Zuera	73%	3	15%	3	15%	3	15%	7
Talamantes	66%	4	17%	6	25%	5	20%	9
Tabuenca	67%	-	-	-	-	-	-	-
Jaulín	66%	-	-	-	-	-	-	-
Fuentes	63%	-	-	-	-	-	-	-

[1] Years between the wildfire and NDVI recovery. [2] Probability of assignment to *P. halepensis* in the year of NDVI recovery. [3] Years between the wildfire and the equalization of assignment probability to *P. halepensis*.

3.4. Spectral Probability of Belonging to P. halepensis as an Indicator of Resilience

Clear differences were observed in the spectral probability of belonging to *P. halepensis* between EU and non-EU samples. As shown in Tables 2 and 3, EU pre-fire samples consistently exhibited probabilities above 78%, whereas non-EU samples remained below 73% across the six analyzed fires, highlighting systematic differences between sampling approaches.

The probability of regenerated vegetation belonging to *P. halepensis* within burned sectors was evaluated at the NDVI recovery year, defined individually for each sample and baseline. In the case of EU samples (Table 2), probabilities were consistently below 40% and in all cases lower than pre-fire values. The non-EU samples (Table 3) showed even lower probabilities, remaining below 25%, further emphasizing the stronger deviation from pre-fire conditions in this sampling approach.

A substantial proportion of EU samples did not recover their pre-fire probability of assignment to *P. halepensis* within the 14-year period, indicating persistent differences in species signal despite recovery in vegetation cover and photosynthetic activity. In EU samples that did recover, this occurred after an average of 12 years. In contrast, among the non-EU samples, three areas never reached pre-fire assignment levels, while the remaining three recovered in less than nine years, indicating a shorter recovery time compared to EU-based sampling.

When analyzing the relationship between post-fire NDVI differences (across multiple baselines) and the annual probability of assignment to *P. halepensis* (Figure 10), results indicated that although NDVI differences tended to stabilize over time, assignment probabilities continued to increase. This relationship followed a consistent logarithmic trend, with coefficients of determination (R^2) ranging from 0.41 to 0.47, regardless of the baseline model applied.

3.5. Verification of Spectral Results Through Floristic Inventories

Field inventories evaluated the recovery of *P. halepensis* and *Q. coccifera* in fires $\leq$ 15 years and >15 years, compared to unburned control areas. For *P. halepensis*, crown cover increased with time since the fire (Figure 11). In fires $\leq$ 15 years old, crown cover was significantly

lower than in controls (p-value = 0.0014); in fires > 15 years, cover remained slightly lower, with no significant differences (p-value = 0.07).

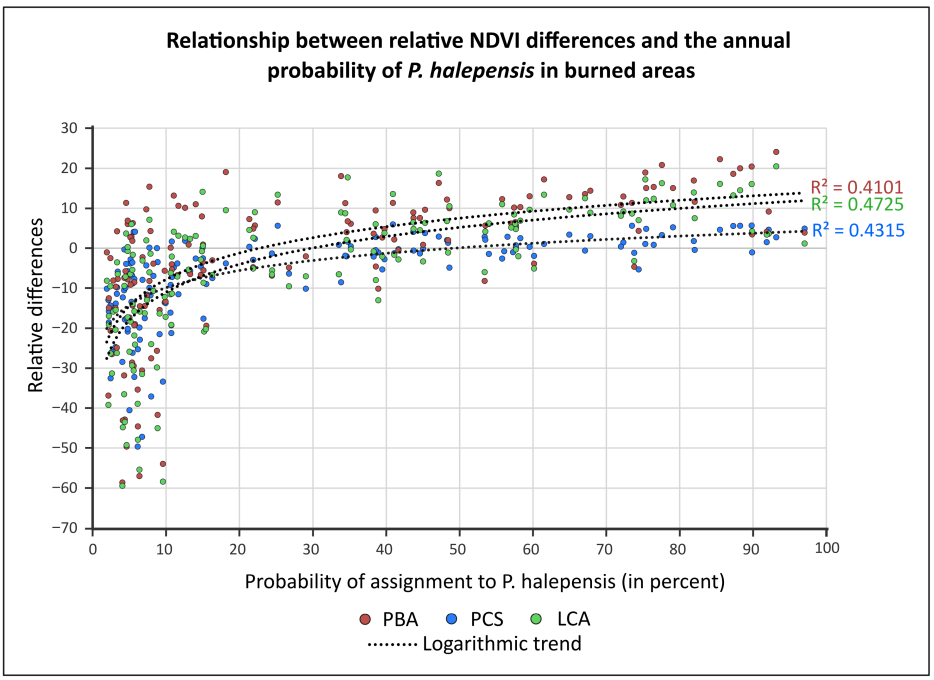

Figure 10. NDVI relative differences vs. *P. halepensis* assignment probability. NDVI relative differences correspond to the difference between the NDVI value of the burned area and the baseline in the same post-fire year. The figure shows this relationship for the three baseline construction approaches within the EUs.

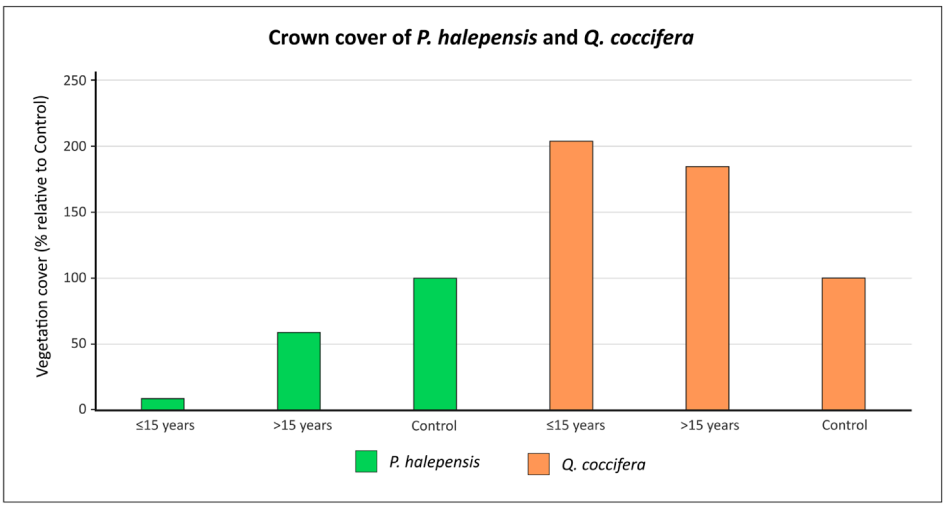

Figure 11. Relative crown area of *P. halepensis* and *Q. coccifera*. Changes in crown area across two post-fire intervals, compared to control plots.

Q. coccifera showed the opposite pattern: during the first 15 years, crown cover was about twice that of the controls (p-value = 0.0001). After more than 15 years, cover decreased progressively and differences with controls were no longer significant (p-value = 0.08). This indicates a structural shift over time, with increasing *P. halepensis* cover and decreasing *Q. coccifera* cover.

Regarding mean height (Figure 12), *P. halepensis* was shorter than controls in both periods: approximately 1 m in fires $\leq$ 15 years and 4 m in >15 years, compared to 7 m in controls. *Q. coccifera* remained stable at around 80 cm with no significant differences.

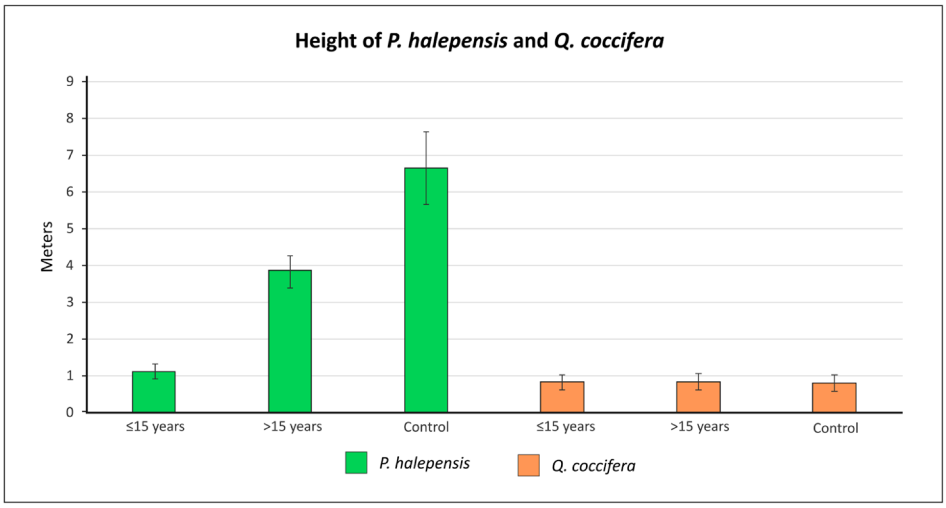

Figure 12. Height of *P. halepensis* and *Q. coccifera*. Individual height across two post-fire time intervals compared to control plots.

Overall, during the first 15 years post-fire, *Q. coccifera* dominated the affected areas, coexisting with *P. halepensis* at approximately 1 m. After 15 years, *P. halepensis* increased in cover and height, although it did not reach the levels observed in unburned plots.

4. Discussion

4.1. Identification of Control Areas Using Object-Oriented Classification Processes

Resilience analysis based on control areas assumes that, in the absence of fire, the affected zone would have retained characteristics similar to those of the control area [103]. Therefore, accurately identifying control areas is essential to ensure robust and valid comparisons.

In this study, GEOBIA was applied to define pre-fire image objects based on spectral, spatial, and contextual characteristics. This method overcomes the limitations of less integrative criteria, such as geographical proximity, isolated biological factors [60,104], or spectral index values [58]. The objects were interpreted as functional ecological units (EUs) and divided by the fire perimeter, allowing the segregation of comparable sectors.

NDVI analysis within each EU showed high pre-fire similarity ($R^2 > 0.8$; bias −0.017–0.039; MAE 0.006–0.043; RMSE 0.008–0.055). Analyses conducted outside the EUs yielded systematically lower NDVI values due to the mixing of spectral signatures from pine formations with different characteristics, reducing the precision of post-fire response assessment. This highlights the value of using GEOBIA-derived EUs to define control areas, improving the coherence and reliability of comparisons.

The study focused on marginal EUs; in fully affected interior zones, equivalent controls could not be defined, requiring additional approaches based on representative external controls. While GEOBIA provides clear advantages in defining ecologically coherent units and improving the precision of post-fire assessments, its computational complexity can pose challenges for large-scale applications. Processing extensive datasets may demand substantial computational resources and time, which could limit its feasibility in very large regions.

4.2. Resilience Through Spectral Indicators (NDVI and Spectral Probability of Belonging to P. halepensis)

When addressing the interpretation of resilience in the context of fire-affected ecosystems, it is essential to take into account its different meanings [105], given its relevance at the research level and in the operational framework of management [46]. One of

the most widespread approaches, that of "engineered resilience", analyzes resilience through the time required for an ecosystem to recover the original equilibrium after a disturbance [106,107]. Nevertheless, as the use of the term resilience has increased [108], the meaning of "ecological resilience" has been integrated [47,109]. The latter recognizes that perturbations can trigger changes that lead to alternative stable states while maintaining functionality [110]. These are distinct but complementary approaches, whose integration is key to understanding resilience as a process that articulates persistence, adaptation, and transformation [45,111]. However, since this study only uses variables derived from spectral information, the engineering definition of resilience is applied due to its greater simplicity.

Furthermore, a quantitative assessment of resilience that takes into account either the engineering or ecological meaning requires comparing the time trajectories of the affected area with a reference area. This comparison uses metrics that accurately capture the time divergences between the two series. Thus, it allows us to estimate the duration and magnitude of the recovery process. This study approached the estimation of *P. halepensis* community resilience from two different properties. On the one hand, it considered the time elapsed from the fire to the recovery of greenness levels, using NDVI as an indicator. On the other hand, it incorporated the probability of spectral assignment to *P. halepensis*, obtained through a supervised classification process. This approach made it possible to integrate both the speed and direction of post-fire change, aligning with a more comprehensive understanding of the engineering meaning of resilience. These indicators have been widely used in numerous studies that analyze resilience in forest communities, demonstrating their usefulness in assessing the response of ecosystems to disturbances such as fires [112–115].

However, it is important to recognize that resilience in forest ecosystems encompasses multiple structural-functional dimensions. In this sense, the vectors used in this study, although useful, only partially represent the complexity of the ecological recovery process.

4.3. The Role of Baselines in Recovery Time Estimation

Regarding the results obtained for NDVI recovery time, no statistically significant differences were observed among the three approaches used to construct the baselines (PBA, LCA, and PCS). This suggests that the method used to construct such lines did not substantially impact spectral recovery time estimates in contexts such as this study. It should be noted, however, that the results derived from each approach show slight variations, attributable to the characteristics of each method, whose strengths and limitations may influence the interpretation of recovery patterns.

The PBA approach has certain limitations associated with its lower temporal coverage, especially in older fires (around the mid-1980s), due to the scarcity of available Landsat images. Furthermore, by exclusively reflecting pre-fire conditions as a reference, this approach may introduce some bias, as the reference state could be set low if such conditions reflect an anomalous state of a conjunctural nature, such as drought situations [116,117], which do not faithfully represent the state of the ecosystem prior to the fire [26].

This approach guarantees consistency in terms of ecological conditions (previous vegetation, edaphic parameters, and morpho-topographic parameters). However, this condition is absent in the other two approaches because it is not limited to the burned sector but has been overcome by selecting homogeneous patches using the GEOBIA algorithm. This guarantees consistency in comparison exercises between sectors. Consequently, the application of the PBA approach would only be justified in those cases where it is not possible to have representative control areas.

Compared to approaches using control areas (LCA and PCS), both of them provide longer data series and higher temporal correspondence with burned areas after the fire.

Since the LCA approach is based on annual composites, it considers the typical phenological behavior of *P. halepensis* in each object, highlighting the seasonal decline during the summer months, while minimizing interannual fluctuations. Of course, this approach is insensitive to the impact of post-fire thermo-hygrometric variations [118], as well as the natural processes of ecosystem growth or degradation. In other words, this static phenological model could introduce systematic deviations from the typical phenology of *P. halepensis*. In addition, it is not able to capture inter-annual variations attributable to particular climatic conditions. For example, favorable weather conditions over the course of a year could cause an accelerated increase in NDVI in both the burned and control areas. However, when the burned area is compared to a stable reference line, a false recovery reading would be generated. Similarly, a dry year could result in an apparent slowing of the recovery process.

By contrast, the PCS approach better reflects the interannual variations associated with photosynthetic activity and allows a more realistic interpretation of the recovery process because it compares the evolution of vegetation between burned and control areas synchronously. This approach captures how thermo-pluviometric conditions affect both zones simultaneously, providing a more accurate context for interpreting relative changes between sectors. Therefore, the PCS approach offers a more complete view of the recovery process of burned areas. However, in the context of resilience analysis, understood as a measure of recovery time, all three approaches (PCS, PBA, and LCA) have been shown to provide similar results. Although PCS is the most appropriate approach, this suggests that PBA and LCA may also be useful, particularly when synchronous analysis is not possible.

4.4. Resilience of P. halepensis Formations

Due to the serotinous nature of its cones, *P. halepensis* is one of the most fire-adapted conifers in the Mediterranean [119]. However, it is frequently affected by fires, which makes quantifying its regeneration patterns necessary [120]. The results allowed the characterization of its phenological cycle, showing maximum NDVI values in winter and spring and minimum values in summer, with a seasonal decrease of about 0.05 units due to summer drought.

The post-fire intra-annual analysis shows that, from the fifth year onward, phenological cycles similar to the baselines begin to appear. Although slight interannual variations persist, there is a clear trend toward stabilization of phenological patterns. However, during the first years after the fire, these differences are more pronounced, as the burned areas are initially colonized by herbaceous vegetation with lower structural complexity and a phenological behavior markedly different from that expected in *P. halepensis* communities.

NDVI recovery times in *P. halepensis* are highly variable due to the interaction of fire severity, climatic conditions, topography, and local floristic composition [57,121,122]. This results in heterogeneous recovery trajectories, even within the same forest.

In general terms, the results indicate that the spectral recovery of NDVI in the analyzed EUs is reached, on average, approximately seven years after the fire. This estimated period is reasonably consistent with other studies using NDVI as an indicator of post-fire recovery. For example, in ecosystems very close to those analyzed in this work, Paci et al. [103] and Vicente-Serrano et al. [123] estimated recovery periods of 10 and 13 years, respectively. In contrast, the analysis based on unadjusted EU samples yields an average of less than six years. This difference suggests a possible underestimation due to the greater spectral heterogeneity of these samples, which is related to the high presence of shrublands.

When the NDVI trajectories of the affected areas converged with their respective baselines, the probability of spectral assignment to *P. halepensis* was generally low (<40%). Although the NDVI levels were similar to the baseline ones, this result suggests that the plant composition does not correspond to the pre-fire *P. halepensis* stands. Rather, these

areas appear to be mixed communities, where pine forests coexist with a Mediterranean shrub understory, which are characterized by a rapid post-fire cover growth [124].

Although the probability of *P. halepensis* presence was low when the NDVI trajectories converged with baselines, it increased significantly after approximately 13 years. The relationship between the evolution of relative NDVI differences and the probability of assignment to *P. halepensis* follows a logarithmic function. This pattern indicates that, although differences in NDVI between burned areas and their corresponding baselines stabilize relatively quickly, the probability of assignment to *P. halepensis* increases steadily over time, as widely documented in the scientific literature. However, numerous areas had not yet reached this level, suggesting that the recovery of *P. halepensis* communities had not generally been reestablished within the observation period. This may represent a shift of the *P. halepensis* forest to an alternative state dominated by shrub species. Such a transition could result from the interplay of multiple factors, including fire severity, post-fire climatic conditions, and the pre-existing structure and composition of the community, which collectively influence its recovery potential and post-fire successional dynamics.

Along these lines, different studies by Trabaud (1998) [125], Broncano et al. [126] and Kazanis et al. [127] determined, using different methodological approaches, that recovery of *P. halepensis* recovery occurs within 10 to 15 years after fire. Numerous studies also agree that the species reaches sexual reproductive maturity from this period onward, allowing the accumulation of a dense crown seed bank sufficient for regeneration after future fires, indicating a certain level of development and recovery of the ecosystem [128–130].

Field floristic inventories show that *P. halepensis* occupation continues to increase 15 years after the fire, with significant differences compared to the control areas. During the first 15 years post-fire, the cover of the burned areas is dominated by shrub species such as *Q. coccifera*, which share the same stratum (about one meter in height) with pine seedlings. Although a high density of pine seedlings is observed in the initial stages [131,132], these communities coexist with an abundant presence of leguminous and herbaceous species from the soil seed bank [133,134], as well as resprouting shrubs. As succession progresses, *P. halepensis* seedlings develop and displace herbaceous and leguminous species progressively, forming an increasingly monospecific community [135]. Field data corroborate this trend, showing a decrease in shrub cover and an increase in pine forest cover 15 years after fire, consistent with spectral assignment probability results.

The temporal discrepancy between the date of convergence of NDVI trajectories and the time at which the corresponding assignment probability is reached suggests that NDVI recovery does not necessarily imply full recovery. This highlights that both indicators reflect complementary dimensions of resilience [136], i.e., on the one hand, the degree of vegetation cover and, on the other hand, the specific composition of plant communities.

It should be noted that the probability of assignment to *P. halepensis* did not recover in any events without convergence in NDVI trajectories. Both indicators are spectral in nature. Although NDVI is a good indicator of the general recovery process [34,137], it is insufficient alone for resilience-focused studies.

In particular, the rapid colonization of burned areas by herbaceous and pioneer species can lead to a relatively fast recovery of NDVI values, which may not correspond to the reestablishment of woody vegetation or ecosystem functionality. In this context, spectral indices incorporating shortwave infrared wavelengths, such as the NBR, have demonstrated enhanced sensitivity to post-fire vegetation dynamics, enabling a more comprehensive characterization of recovery processes [138,139].

The results support the hypothesis that NDVI alone cannot comprehensively assess post-fire community resilience. Its analysis must be complemented with indicators addressing structural, functional, and compositional aspects.

In general, results indicate that *P. halepensis* communities in the Aragon region present a good level of post-fire resilience. In most of the analyzed events, the recovery levels align with those described in the literature for other Mediterranean areas [130,140–145]. However, the heterogeneity observed in the regeneration patterns highlights the diversity of ecological scenarios and local dynamics. These findings may help identify areas where *P. halepensis* is likely to regenerate poorly, guiding targeted restoration or mitigation efforts.

4.5. Future Lines

The analysis highlighted new research directions, including extending the study to other tree communities to enable comparisons across forest formations and improve the general understanding of forest resilience. It is also emphasized that incorporating additional analytical dimensions, including new spectral indices (e.g., red-edge and SWIR-based indices) and thermal variables, as well as biophysical variables related to carbon recovery or the restoration of hydrological function, is important for a more accurate and multi-scale assessment of resilience. Finally, investigating the relationship between EUs with representative control areas and those entirely affected by fire is crucial to achieve a more integrated understanding of forest fire dynamics.

5. Conclusions

The results obtained from the analysis of resilience in *P. halepensis* communities allow the following conclusions:

- The GEOBIA algorithm proved to be an effective tool for delineating ecological units (EUs), enabling accurate segmentation based on spectral, spatial, and contextual characteristics. This approach facilitates the simultaneous segmentation of burned and unaffected sectors, making it a suitable method for selecting representative control areas by minimizing the spatial uncertainty typically associated with this type of analysis.
- The PCS baseline (Post-fire Control Synchronous), constructed using external controls and synchronous data, provides a more comprehensive and adjusted perspective of the post-fire regeneration by integrating interannual phenological variability. However, no statistically significant differences were found in NDVI recovery time estimates among the different baselines.
- On average, the NDVI in *P. halepensis* communities recovers seven years after a fire. Even before then, phenological patterns similar to pre-fire conditions are evident. However, at that time the probability of presence of *P. halepensis* is still low (<40%) due to the dominance of shrubs such as *Q. coccifera* and other pioneer species. Field inventories confirm that at least 15 years are required for these communities to be replaced by monospecific pine forests that reach values comparable to the reference ones. These dynamics confirm the high resilience of *P. halepensis* in Mediterranean environments, although the heterogeneity among EUs highlights the importance of local post-fire management.
- The temporal difference between NDVI recovery and the probability of assignment to *P. halepensis* indicates that, while NDVI is useful as a preliminary indicator, it is insufficient for assessing tree communities. NDVI recovery does not necessarily imply restoration of the original tree composition. Since both indicators capture different dimensions—vegetation cover versus species composition—it is clear that integrating complementary metrics is essential for a comprehensive assessment of resilience in tree communities.

Author Contributions: Conceptualization, P.M.-O. and F.P.-C.; methodology, P.M.-O., C.I. and D.B.A.; software, P.M.-O., C.I. and D.B.A.; validation, F.P.-C. and R.M.; formal analysis, P.M.-O.; investigation, P.M.-O. and F.P.-C.; resources, F.P.-C. and R.M.; data curation, P.M.-O.; writing—original draft preparation, P.M.-O.; writing—review and editing, P.M.-O., F.P.-C. and R.M.; visualization, P.M.-O.; supervision, F.P.-C. and R.M.; project administration, P.M.-O. and F.P.-C.; funding acquisition, F.P.-C. and R.M. All authors have read and agreed to the published version of the manuscript.

Funding: This research was funded by the Government of Aragón through the program "Ayudas para la Contratación de Personal Investigador Predoctoral (2024–2028)", funded under ORDEN ECU/592/2024. Additional support was provided by the I+D+i project "Dynamic analysis of the resilience of Fire Affected Forest Landscapes (PaF) using multisensor spectral indicators" (PID2020-118886RB-I00), funded by the Ministry of Science, Innovation and Universities of the Government of Spain and by the I+D+i project "Remote and proximal sensing for modelling and monitoring soil recovery in burned areas (Sens4Soil)" (PID2024-160889OA-I00) funded by the Ministry of Science, Innovation and Universities of the Government of Spain.

Data Availability Statement: The data supporting the findings of this study are publicly available in Zenodo at https://doi.org/10.5281/zenodo.17183984.

Acknowledgments: The authors would like to acknowledge the support provided by the "Fundação Cearense de Apoio ao Desenvolvimento Científico e Tecnológico" (FUNCAP, process number BP6-00241-00158.01.00/25) as a research productivity fellowship provided for the fourth author.

Conflicts of Interest: The authors declare no conflicts of interest.

Abbreviations

The following abbreviations are used in this manuscript:

PBA	Pre-fire Burned Annual composite
PCS	Post-fire Control Synchronous
LCA	Long-term Control Annual composite
EU	Ecological Unit
Non-EU	Non-Ecological Unit

Appendix A

This appendix includes supplementary information that allows the characterization of burned areas both from a topographic perspective, using elevation data derived from Digital Terrain Models provided by the Centro Nacional de Información Geográfica (CNIG), and in terms of fire severity, assessed through spectral indices (dNBR and RdNBR).

Table A1. Topographic and fire severity metrics of the analyzed burned areas.

	Elevation				**dNBR**				**RdNBR**			
	Mean	**SD**	**Max**	**Min**	**Mean**	**SD**	**Max**	**Min**	**Mean**	**SD**	**Max**	**Min**
Riglos	879.90	215.64	1365.98	461.35	609.96	288.69	1233.26	−284.65	860.24	361.90	3258.33	−367.07
Zuera	560.65	55.99	677.29	395.49	515.48	238.10	1000.19	−290.40	875.91	331.98	2417.37	−360.32
Talamantes	906.83	40.78	983.12	813.02	468.55	101.82	724.80	−281.05	635.72	212.97	1141.31	−368.44
Tabuenca	779.02	79.58	1093.43	699.83	535.15	262.66	976.862	−284.33	878.84	238.69	2510.12	−370.48
Jaulín	650.98	35.77	544.63	718.56	574.45	231.34	1009.72	−281.64	925.02	330.67	3585.35	−361.85
Fuentes	807.85	65.80	937.29	676.26	620.00	295.10	1310.45	−285.80	880.75	360.20	3450.80	−368.90

Appendix B

This appendix provides a detailed summary of the number of samples used for each vegetation class in both the training and test datasets. It includes all land cover categories considered in the supervised classification process.

Table A2. Distribution of training and test samples used for vegetation classification.

Label	Test Dataset Count	Train Dataset Count
Bare soil	20	47
Pinus halepensis	70	164
Pinus sylvestris	65	151
Shrub Pinus sylvestris	49	115
Quercus ilex	34	78
Pinus nigra	27	64
Shrub of Pinus nigra	25	59
Quercus g. cerrioides	23	54
Shrub of Pinus halepensis	23	52
Shrub of Pinus pinaster	18	40
Shrub of Quercus ilex	15	36
Pinus pinaster	12	28
Shrub of Quercus g. cerrioides	10	24

Appendix C

This appendix summarizes the variables used across the different methodological steps of the study, including vegetation mapping and object-based image classification. It indicates which variables were applied in each stage of the analysis, covering spectral, topographic, and environmental information derived from Landsat imagery and ancillary datasets.

Table A3. Variables used in vegetation mapping and image segmentation processes.

Variables	2.3. Vegetation Mapping	2.4. Image Segmentation and Object-Based Classification
Landsat spectral bands (blue, green, red, NIR, SWIR1, SWIR2)	X	X
Normalized Difference Vegetation Index (NDVI)	X	X
Altitude	X	
Relief shading	X	
Lithology	X	
Bare Soil Index (BSI)		X

References

1. Scott, A.C. The Pre-Quaternary History of Fire. *Palaeogeogr. Palaeoclimatol. Palaeoecol.* **2000**, *164*, 281–329. [CrossRef]
2. Pausas, J.G.; Llovet, J.; Rodrigo, A.; Vallejo, R. Are Wildfires a Disaster in the Mediterranean Basin? A Review. *Int. J. Wildl. Fire* **2008**, *17*, 713–723. [CrossRef]
3. Ursino, N.; Romano, N. Wild Forest Fire Regime Following Land Abandonment in the Mediterranean Region. *Geophys. Res. Lett.* **2014**, *41*, 8359–8368. [CrossRef]
4. Pausas, J.G.; Keeley, J.E. Abrupt Climate-Independent Fire Regime Changes. *Ecosystems* **2014**, *17*, 1109–1120. [CrossRef]
5. Dupuy, J.L.; Fargeon, H.; Martin-StPaul, N.; Pimont, F.; Ruffault, J.; Guijarro, M.; Hernando, C.; Madrigal, J.; Fernandes, P. Climate Change Impact on Future Wildfire Danger and Activity in Southern Europe: A Review. *Ann. For. Sci.* **2020**, *77*, 35. [CrossRef]
6. Abatzoglou, J.T.; Williams, A.P.; Boschetti, L.; Zubkova, M.; Kolden, C.A. Global Patterns of Interannual Climate–Fire Relationships. *Glob. Change Biol.* **2018**, *24*, 5164–5175. [CrossRef]
7. Nolan, R.H.; Collins, L.; Leigh, A.; Ooi, M.K.J.; Curran, T.J.; Fairman, T.A.; Resco de Dios, V.; Bradstock, R. Limits to Post-Fire Vegetation Recovery under Climate Change. *Plant Cell Environ.* **2021**, *44*, 3471–3489. [CrossRef] [PubMed]
8. Chavardès, R.D.; Daniels, L.D. Altered Mixed-Severity Fire Regime Has Homogenised Montane Forests of Jasper National Park. *Int. J. Wildl. Fire* **2016**, *25*, 433–444. [CrossRef]
9. Lecina-Diaz, J.; Martínez-Vilalta, J.; Alvarez, A.; Vayreda, J.; Retana, J. Assessing the Risk of Losing Forest Ecosystem Services Due to Wildfires. *Ecosystems* **2021**, *24*, 1687–1701. [CrossRef]

10. Neary, D.G.; Klopatek, C.C.; DeBano, L.F.; Ffolliott, P.F. Fire Effects on Belowground Sustainability: A Review and Synthesis. *For. Ecol. Manag.* **1999**, *122*, 51–71. [CrossRef]
11. Keeley, J.E.; Pausas, J.G.; Rundel, P.W.; Bond, W.J.; Bradstock, R.A. Fire as an Evolutionary Pressure Shaping Plant Traits. *Trends Plant Sci.* **2011**, *16*, 406–411. [CrossRef]
12. Pausas, J.G. Generalized Fire Response Strategies in Plants and Animals. *Oikos* **2019**, *128*, 147–153. [CrossRef]
13. Keeley, J.E. Reproductive Cycles and Fire Regimes. In *Fire Regimes and Ecosystem Properties: Proceedings of the Conference, December 11–15, 1978, Honolulu, Hawaii*; Mooney, H.A., Bonnicksen, T.M., Christensen, N.L., Jr., Lotan, J.E., Reiners, W.A., Eds.; USDA Forest Service General Technical Report WO-GTR-26; United States Forest Service: Washington, DC, USA, 1981; pp. 231–277.
14. Pausas, J.G.; Keeley, J.E.; Schwilk, D.W. Flammability as an Ecological and Evolutionary Driver. *J. Ecol.* **2017**, *105*, 289–297. [CrossRef]
15. Ojeda, F.; Brun, F.G.; Vergara, J.J. Fire, Rain and the Selection of Seeder and Resprouter Life-Histories in Fire-Recruiting, Woody Plants. *New Phytol.* **2005**, *168*, 155–165. [CrossRef] [PubMed]
16. Bond, W.J.; Midgley, J.J. The Evolutionary Ecology of Sprouting in Woody Plants. *Int. J. Plant Sci.* **2003**, *164*, S103–S114. [CrossRef] [PubMed]
17. Keeley, J.E. Ecology and Evolution of Pine Life Histories. *Ann. For. Sci.* **2012**, *69*, 445–453. [CrossRef]
18. Daskalakou, E.N.; Thanos, C.A. Aleppo Pine (*Pinus halepensis*) Postfire Regeneration: The Role of Canopy and Soil Seed Banks. *Int. J. Wildl. Fire* **1996**, *6*, 59–66. [CrossRef]
19. Moya, D.; González-De Vega, S.; García-Orenes, F.; Morugán-Coronado, A.; Arcenegui, V.; Mataix-Solera, J.; Lucas-Borja, M.E.; De las Heras, J. Temporal Characterisation of Soil-Plant Natural Recovery Related to Fire Severity in Burned *Pinus halepensis* Mill. Forests. *Sci. Total Environ.* **2018**, *640–641*, 42–51. [CrossRef]
20. Calvo, L.; Santalla, S.; Valbuena, L.; Marcos, E.; Tárrega, R.; Luis-Calabuig, E. Post-Fire Natural Regeneration of a Pinus Pinaster Forest in NW Spain. *Plant Ecol.* **2008**, *197*, 81–90. [CrossRef]
21. Moya, D.; Saracino, A.; Salvatore, R.; Lovreglio, R.; De Las Heras, J.; Leone, V. Anatomic Basis and Insulation of Serotinous Cones in *Pinus halepensis* Mill. *Trees Struct. Funct.* **2008**, *22*, 511–519. [CrossRef]
22. Fernández, C.; Vega, J.A.; Fonturbel, T.; Jiménez, E.; Pérez-Gorostiaga, P. Effects of Wildfire, Salvage Logging and Slash Manipulation on Pinus Pinaster Ait. Recruitment in Orense (NW Spain). *For. Ecol. Manag.* **2008**, *255*, 1294–1304. [CrossRef]
23. García-Llamas, P.; Suárez-Seoane, S.; Taboada, A.; Fernández-Manso, A.; Quintano, C.; Fernández-García, V.; Fernández-Guisuraga, J.M.; Marcos, E.; Calvo, L. Environmental Drivers of Fire Severity in Extreme Fire Events That Affect Mediterranean Pine Forest Ecosystems. *For. Ecol. Manag.* **2019**, *433*, 24–32. [CrossRef]
24. Chuvieco, E.; Aguado, I.; Salas, J.; García, M.; Yebra, M.; Oliva, P. Satellite Remote Sensing Contributions to Wildland Fire Science and Management. *Curr. For. Rep.* **2020**, *6*, 81–96. [CrossRef]
25. Zang, J.; Qiu, F.; Zhang, Y.; Shang, R. A Dataset of Forest Regrowth in Globally Key Deforestation Regions. *Sci. Data* **2025**, *12*, 154. [CrossRef]
26. McKenna, P.B.; Phinn, S.R.; Erskine, P.D. Fire Resilience Analysis: Using High Temporal and Spatial Satellite Imagery for Rehabilitated Landscapes. *Ecol. Eng.* **2024**, *212*, 107478. [CrossRef]
27. Bright, B.C.; Hudak, A.T.; Kennedy, R.E.; Braaten, J.D.; Henareh Khalyani, A. Examining Post-Fire Vegetation Recovery with Landsat Time Series Analysis in Three Western North American Forest Types. *Fire Ecol.* **2019**, *15*, 8. [CrossRef]
28. Morresi, D.; Vitali, A.; Urbinati, C.; Garbarino, M. Forest Spectral Recovery and Regeneration Dynamics in Stand-Replacing Wildfires of Central Apennines Derived from Landsat Time Series. *Remote Sens.* **2019**, *11*, 308. [CrossRef]
29. Hislop, S.; Haywood, A.; Jones, S.; Soto-Berelov, M.; Skidmore, A.; Nguyen, T.H. A Satellite Data Driven Approach to Monitoring and Reporting Fire Disturbance and Recovery across Boreal and Temperate Forests. *Int. J. Appl. Earth Obs. Geoinf.* **2020**, *87*, 102034. [CrossRef]
30. Wulder, M.A.; White, J.C.; Loveland, T.R.; Woodcock, C.E.; Belward, A.S.; Cohen, W.B.; Fosnight, E.A.; Shaw, J.; Masek, J.G.; Roy, D.P. The Global Landsat Archive: Status, Consolidation, and Direction. *Remote Sens. Environ.* **2016**, *185*, 271–283. [CrossRef]
31. Kennedy, R.E.; Andréfouët, S.; Cohen, W.B.; Gómez, C.; Griffiths, P.; Hais, M.; Healey, S.P.; Helmer, E.H.; Hostert, P.; Lyons, M.B.; et al. Bringing an Ecological View of Change to Landsat-Based Remote Sensing. *Front. Ecol. Environ.* **2014**, *12*, 339–346. [CrossRef]
32. Zhu, Z. Change Detection Using Landsat Time Series: A Review of Frequencies, Preprocessing, Algorithms, and Applications. *ISPRS J. Photogramm. Remote Sens.* **2017**, *130*, 370–384. [CrossRef]
33. Ibarra-Bonilla, J.S.; Pinedo-Alvarez, A.; Prieto-Amparán, J.A.; Siller-Clavel, P.; Santellano-Estrada, E.; Álvarez-Holguín, A.; Villarreal-Guerrero, F. Post-Fire Vegetation Dynamics of a Temperate Mixed Forest: An Assessment Based on the Variability of Landsat Spectral Indices. *Trees For. People* **2024**, *17*, 100648. [CrossRef]
34. Viedma, O.; Meliá, J.; Segarra, D.; García-Haro, J. Modeling Rates of Ecosystem Recovery after Fires by Using Landsat TM Data. *Remote Sens. Environ.* **1997**, *61*, 383–398. [CrossRef]
35. Storey, E.A.; Stow, D.A.; Roberts, D.A. Evaluating Uncertainty in Landsat-Derived Postfire Recovery Metrics Due to Terrain, Soil, and Shrub Type Variations in Southern California. *GIScience Remote Sens.* **2020**, *57*, 352–368. [CrossRef] [PubMed]

36. Blackburn, G.A.; Milton, E.J. Seasonal Variations in the Spectral Reflectance of Deciduous Tree Canopies. *Int. J. Remote Sens.* **1995**, *16*, 709–720. [CrossRef]
37. Khormizi, H.Z.; Malamiri, H.R.G.; Kalantari, Z.; Ferreira, C.S.S. Trend of Changes in Phenological Components of Iran's Vegetation Using Satellite Observations. *Remote Sens.* **2023**, *15*, 4468. [CrossRef]
38. Kurbanov, E.; Vorobev, O.; Lezhnin, S.; Sha, J.; Wang, J.; Li, X.; Cole, J.; Dergunov, D.; Wang, Y. Remote Sensing of Forest Burnt Area, Burn Severity, and Post-Fire Recovery: A Review. *Remote Sens.* **2022**, *14*, 4714. [CrossRef]
39. Hislop, S.; Jones, S.; Soto-Berelov, M.; Skidmore, A.; Haywood, A.; Nguyen, T.H. Using Landsat Spectral Indices in Time-Series to Assess Wildfire Disturbance and Recovery. *Remote Sens.* **2018**, *10*, 460. [CrossRef]
40. White, J.C.; Wulder, M.A.; Hermosilla, T.; Coops, N.C.; Hobart, G.W. A Nationwide Annual Characterization of 25 Years of Forest Disturbance and Recovery for Canada Using Landsat Time Series. *Remote Sens. Environ.* **2017**, *194*, 303–321. [CrossRef]
41. Celebrezze, J.V.; Franz, M.C.; Andrus, R.A.; Stahl, A.T.; Steen-Adams, M.; Meddens, A.J.H. A Fast Spectral Recovery Does Not Necessarily Indicate Post-Fire Forest Recovery. *Fire Ecol.* **2024**, *20*, 54. [CrossRef]
42. Bartels, S.F.; Chen, H.Y.H.; Wulder, M.A.; White, J.C. Trends in Post-Disturbance Recovery Rates of Canada's Forests Following Wildfire and Harvest. *For. Ecol. Manag.* **2016**, *361*, 194–207. [CrossRef]
43. Westman, W.E.; O'Leary, J.F. Measures of Resilience: The Response of Coastal Sage Scrub to Fire. *Vegetatio* **1986**, *65*, 179–189. [CrossRef]
44. Wessels, K.J.; Prince, S.D.; Carroll, M.; Malherbe, J. Relevance of Rangeland Degradation in Semiarid Northeastern South Africa to the Nonequilibrium Theory. *Ecol. Appl.* **2007**, *17*, 815–827. [CrossRef]
45. Hodgson, D.; McDonald, J.L.; Hosken, D.J. What Do You Mean, "Resilient"? *Trends Ecol. Evol.* **2015**, *30*, 503–506. [CrossRef]
46. Marcos, B.; Gonçalves, J.; Alcaraz-Segura, D.; Cunha, M.; Honrado, J.P. Assessing the Resilience of Ecosystem Functioning to Wildfires Using Satellite-Derived Metrics of Post-Fire Trajectories. *Remote Sens. Environ.* **2023**, *286*, 113441. [CrossRef]
47. Falk, D.A.; van Mantgem, P.J.; Keeley, J.E.; Gregg, R.M.; Guiterman, C.H.; Tepley, A.J.; Young, D.J.; Marshall, L.A. Mechanisms of Forest Resilience. *For. Ecol. Manag.* **2022**, *512*, 120129. [CrossRef]
48. Johnstone, J.F.; Allen, C.D.; Franklin, J.F.; Frelich, L.E.; Harvey, B.J.; Higuera, P.E.; Mack, M.C.; Meentemeyer, R.K.; Metz, M.R.; Perry, G.L.W.; et al. Changing Disturbance Regimes, Ecological Memory, and Forest Resilience. *Front. Ecol. Environ.* **2016**, *14*, 369–378. [CrossRef]
49. Huerta, S.; Marcos, E.; Fernández-García, V.; Calvo, L. Resilience of Mediterranean Communities to Fire Depends on Burn Severity and Type of Ecosystem. *Fire Ecol.* **2022**, *18*, 28. [CrossRef]
50. Singh, S.S.; Jeganathan, C. Quantifying Forest Resilience Post Forest Fire Disturbances Using Time-Series Satellite Data. *Environ. Monit. Assess.* **2024**, *196*, 26. [CrossRef]
51. Ingrisch, J.; Bahn, M. Towards a Comparable Quantification of Resilience. *Trends Ecol. Evol.* **2018**, *33*, 251–259. [CrossRef]
52. Van Meerbeek, K.; Jucker, T.; Svenning, J.C. Unifying the Concepts of Stability and Resilience in Ecology. *J. Ecol.* **2021**, *109*, 3114–3132. [CrossRef]
53. Hartung, M.; Carreño-Rocabado, G.; Peña-Claros, M.; van der Sande, M.T. Tropical Dry Forest Resilience to Fire Depends on Fire Frequency and Climate. *Front. For. Glob. Change* **2021**, *4*, 755104. [CrossRef]
54. Jones, L.P.; Turvey, S.T.; Massimino, D.; Papworth, S.K. Investigating the Implications of Shifting Baseline Syndrome on Conservation. *People Nat.* **2020**, *2*, 1131–1144. [CrossRef]
55. Hernández-Clemente, R.; Navarro Cerrillo, R.M.; Gitas, I.Z. Monitoring Post-Fire Regeneration in Mediterranean Ecosystems by Employing Multitemporal Satellite Imagery. *Int. J. Wildl. Fire* **2009**, *18*, 648–658. [CrossRef]
56. Labenski, P.; Millin-Chalabi, G.; Pacheco-Pascagaza, A.M.; Senn, J.A.; Fassnacht, F.E.; Clay, G.D. An Optical Satellite-Based Analysis of Phenology and Post-Fire Vegetation Recovery in UK Upland Moorlands. *Environ. Sustain. Indic.* **2024**, *24*, 100492. [CrossRef]
57. Shen, Y.; Prentice, I.C.; Harrison, S.P. Investigation of Factors That Affect Post-Fire Recovery of Photosynthetic Activity at Global Scale. *Ecol. Indic.* **2025**, *171*, 113206. [CrossRef]
58. Díaz-Delgado, R.; Salvador, R.; Pons, X. Monitoring of Plant Community Regeneration after Fire by Remote Sensing. In *Fire Management and Landscape Ecology*; Trabaud, L., Ed.; International Association of Wildland Fire: Fairfield, WA, USA, 1998; pp. 315–324.
59. Di Mauro, B.; Fava, F.; Busetto, L.; Crosta, G.F.; Colombo, R. Post-Fire Resilience in the Alpine Region Estimated from MODIS Satellite Multispectral Data. *Int. J. Appl. Earth Obs. Geoinf.* **2014**, *32*, 163–172. [CrossRef]
60. Gemitzi, A.; Koutsias, N. Assessment of Properties of Vegetation Phenology in Fire-Affected Areas from 2000 to 2015 in the Peloponnese, Greece. *Remote Sens. Appl. Soc. Environ.* **2021**, *23*, 100535. [CrossRef]
61. Lhermltte, S.; Verbesselt, J.; Verstraeten, W.W.; Coppin, P. A Pixel Based Regeneration Index Using Time Series Similarity and Spatial Context. *Photogramm. Eng. Remote Sens.* **2010**, *76*, 673–682. [CrossRef]
62. Landi, M.A.; Ojeda, S.; di Bella, C.M.; Salvatierra, P.; Argañaraz, J.P.; Bellis, L.M. Selección de Parcelas Control Para Estudios de La Dinámica Post-Incendio: Desempeño de Rutinas No Paramétricas y Autorregresivas. *Rev. Teledetec.* **2017**, *2017*, 79–90. [CrossRef]

63. Hay, G.J.; Castilla, G. Geographic Object-Based Image Analysis (GEOBIA): A New Name for a New Discipline. In *Object-Based Image Analysis*; Lecture Notes in Geoinformation and Cartography; Springer: Berlin/Heidelberg, Germany, 2008; pp. 75–89. [CrossRef]
64. Köppen, W. Versuch Einer Klassifikation Der Klimate, Vorzugsweise Nach Ihren Beziehungen Zur Pflanzenwelt. *Geogr. Z.* **1900**, *6*, 593–611.
65. Key, C.H.; Benson, N.C. Landscape Assessment (LA) Sampling and Analysis Methods. In *FIREMON: Fire Effects Monitoring and Inventory System*; General Technical Report RMRS-GTR-164-CD; USDA Forest Service: Hilo, HI, USA, 2006.
66. Miller, J.D.; Thode, A.E. Quantifying Burn Severity in a Heterogeneous Landscape with a Relative Version of the Delta Normalized Burn Ratio (DNBR). *Remote Sens. Environ.* **2007**, *109*, 66–80. [CrossRef]
67. Alves, D.B.; Fidelis, A.; Pérez-Cabello, F.; Alvarado, S.T.; Conciani, D.E.; Cambraia, B.C.; da Silveira, A.L.P.; Silva, T.S.F. Impact of Image Acquisition Lag-Time on Monitoring Short-Term Postfire Spectral Dynamics in Tropical Savannas: The Campos Amazônicos Fire Experiment. *J. Appl. Remote Sens.* **2022**, *16*, 034507. [CrossRef]
68. Granger, B.E.; Perez, F. Jupyter: Thinking and Storytelling with Code and Data. *Comput. Sci. Eng.* **2021**, *23*, 7–14. [CrossRef]
69. Gorelick, N.; Hancher, M.; Dixon, M.; Ilyushchenko, S.; Thau, D.; Moore, R. Google Earth Engine: Planetary-Scale Geospatial Analysis for Everyone. *Remote Sens. Environ.* **2017**, *202*, 18–27. [CrossRef]
70. Wilson, R.T. Py6S: A Python Interface to the 6S Radiative Transfer Model. *Comput. Geosci.* **2013**, *51*, 166–171. [CrossRef]
71. Scheffler, D.; Hollstein, A.; Diedrich, H.; Segl, K.; Hostert, P. AROSICS: An Automated and Robust Open-Source Image Co-Registration Software for Multi-Sensor Satellite Data. *Remote Sens.* **2017**, *9*, 676. [CrossRef]
72. Roy, D.P.; Zhang, H.K.; Ju, J.; Gomez-Dans, J.L.; Lewis, P.E.; Schaaf, C.B.; Sun, Q.; Li, J.; Huang, H.; Kovalskyy, V. A General Method to Normalize Landsat Reflectance Data to Nadir BRDF Adjusted Reflectance. *Remote Sens. Environ.* **2016**, *176*, 255–271. [CrossRef]
73. Soenen, S.A.; Peddle, D.R.; Coburn, C.A. SCS+C: A Modified Sun-Canopy-Sensor Topographic Correction in Forested Terrain. *IEEE Trans. Geosci. Remote Sens.* **2005**, *43*, 2148–2159. [CrossRef]
74. Scheffler, D.; Frantz, D.; Segl, K. Spectral Harmonization and Red Edge Prediction of Landsat-8 to Sentinel-2 Using Land Cover Optimized Multivariate Regressors. *Remote Sens. Environ.* **2020**, *241*, 111723. [CrossRef]
75. Belda, S.; Pipia, L.; Morcillo-Pallarés, P.; Rivera-Caicedo, J.P.; Amin, E.; De Grave, C.; Verrelst, J. DATimeS: A Machine Learning Time Series GUI Toolbox for Gap-Filling and Vegetation Phenology Trends Detection. *Environ. Model. Softw.* **2020**, *127*, 104666. [CrossRef]
76. Nguyen, M.D.; Baez-Villanueva, O.M.; Bui, D.D.; Nguyen, P.T.; Ribbe, L. Harmonization of Landsat and Sentinel 2 for Crop Monitoring in Drought Prone Areas: Case Studies of Ninh Thuan (Vietnam) and Bekaa (Lebanon). *Remote Sens.* **2020**, *12*, 281. [CrossRef]
77. Murphy, S. Atmospheric Correction of a (Single) Sentinel 2 Image. 2020. Available online: https://github.com/samsammurphy/gee-atmcorr-S2/blob/master/jupyer_notebooks/sentinel2_atmospheric_correction.ipynb (accessed on 9 March 2026).
78. Poortinga, A.; Tenneson, K.; Shapiro, A.; Nquyen, Q.; Aung, K.S.; Chishtie, F.; Saah, D. Mapping Plantations in Myanmar by Fusing Landsat-8, Sentinel-2 and Sentinel-1 Data along with Systematic Error Quantification. *Remote Sens.* **2019**, *11*, 831. [CrossRef]
79. European Space Agency. *Copernicus Global Digital Elevation Model*; European Space Agency: Paris, Frence, 2024. [CrossRef]
80. Rouse, J.W.; Haas, R.H.; Schell, J.A.; Deering, D.W. Monitoring Vegetation Systems in the Great Plains with ERTS. In *3d ERTS-1 Symposium, Volume 1, Section A*; NASA, Goddard Space Flight Center: Greenbelt, MD, USA, 1974.
81. Rikimaru, A.; Roy, P.; Miyatake, S. Tropical Forest Cover Density Mapping. *Trop. Ecol.* **2002**, *43*, 39–47.
82. Eilers, P.H.C. A Perfect Smoother. *Anal. Chem.* **2003**, *75*, 3631–3636. [CrossRef] [PubMed]
83. Savitzky, A.; Golay, M.J.E. Smoothing and Differentiation of Data by Simplified Least Squares Procedures. *Anal. Chem.* **1964**, *36*, 1627–1639. [CrossRef]
84. Iranzo Cubel, C.; Acosta-Ruiz, A.; Montorio Llovería, R.; Hoffren, R.; Pérez-Cabello, F. Evaluación de La Maleabilidad de Los Paisajes Forestales Afectados Por El Fuego En Aragón. In *Geografía: Cambios, Retos y Adaptación: Libro de Actas. XXVIII Congreso de la Asociación Española de Geografía, Logroño*; Asociación Española de Geografía: Madrid, Spain, 2023; Volume 174, pp. 165–174. [CrossRef]
85. Pedregosa, F.; Varoquaux, G.; Gramfort, A.; Michel, V.; Thirion, B.; Grisel, O.; Blondel, M.; Müller, A.; Nothman, J.; Louppe, G.; et al. Scikit-Learn: Machine Learning in Python. *J. Mach. Learn. Res.* **2011**, *12*, 2825–2830. [CrossRef]
86. Lemaître, G.; Nogueira, F.; Aridas, C.K. Imbalanced-Learn: A Python Toolbox to Tackle the Curse of Imbalanced Datasets in Machine Learning. *J. Mach. Learn. Res.* **2017**, *18*, 1–5.
87. Chawla, N.V.; Bowyer, K.W.; Hall, L.O.; Kegelmeyer, W.P. SMOTE: Synthetic Minority Over-Sampling Technique. *J. Artif. Intell. Res.* **2002**, *16*, 321–357. [CrossRef]
88. He, H.; Bai, Y.; Garcia, E.A.; Li, S. ADASYN: Adaptive Synthetic Sampling Approach for Imbalanced Learning. In *2008 IEEE International Joint Conference on Neural Networks*; IEEE: New York, NY, USA, 2008; pp. 1322–1328. [CrossRef]

89. Tomek, I. Two modifications of CNN. *IEEE Trans. Syst. Man Cybern.* **1976**, *SMC-6*, 769–772. [CrossRef]
90. Breiman, L. Random Forests. *Mach. Learn.* **2001**, *45*, 5–32. [CrossRef]
91. Cortes, C.; Vapnik, V.; Saitta, L. Support-Vector Networks. *Mach. Learn.* **1995**, *20*, 273–297. [CrossRef]
92. Maxwell, A.E.; Warner, T.A.; Fang, F. Implementation of Machine-Learning Classification in Remote Sensing: An Applied Review. *Int. J. Remote Sens.* **2018**, *39*, 2784–2817. [CrossRef]
93. Cawley, G.C.; Talbot, N.L.C. On Over-Fitting in Model Selection and Subsequent Selection Bias in Performance Evaluation. *J. Mach. Learn. Res.* **2010**, *11*, 2079–2107.
94. Tassi, A.; Vizzari, M. Object-Oriented Lulc Classification in Google Earth Engine Combining Snic, Glcm, and Machine Learning Algorithms. *Remote Sens.* **2020**, *12*, 3776. [CrossRef]
95. Crowley, M.A.; Cardille, J.A.; White, J.C.; Wulder, M.A. Generating Intra-Year Metrics of Wildfire Progression Using Multiple Open-Access Satellite Data Streams. *Remote Sens. Environ.* **2019**, *232*, 111295. [CrossRef]
96. Achanta, R.; Süsstrunk, S. Superpixels and Polygons Using Simple Non-Iterative Clustering. In *2017 IEEE Conference on Computer Vision and Pattern Recognition (CVPR)*; IEEE: New York, NY, USA, 2017; pp. 4895–4904. [CrossRef]
97. Kruse, F.A.; Lefkoff, A.B.; Boardman, J.W.; Heidebrecht, K.B.; Shapiro, A.T.; Barloon, P.J.; Goetz, A.F.H. The Spectral Image Processing System (SIPS)—Interactive Visualization and Analysis of Imaging Spectrometer Data. *Remote Sens. Environ.* **1993**, *44*, 145–163. [CrossRef]
98. Wang, M.; Huang, Z.; Zhang, X.; Zhang, Y.; Chen, M. Altered Mineral Mapping Based on Ground-Airborne Hyperspectral Data and Wavelet Spectral Angle Mapper Tri-Training Model: Case Studies from Dehua-Youxi-Yongtai Ore District, Central Fujian, China. *Int. J. Appl. Earth Obs. Geoinf.* **2021**, *102*, 102409. [CrossRef]
99. Yi, J.L.R.; Shimabukuro, Y.E.; Quintanilha, J.A. Identificação e Mapeamento de Áreas de Milho Na Região Sul Do Brasil Utilizando Imagens MODIS. *Eng. Agríc.* **2007**, *27*, 753–763. [CrossRef]
100. Vicente, L.E.; Gomesdaniel, D.; Victoria, D.D.C.; Garçon, E.A.M.; Bolf, E.L.; Andrade, R.G.; Da Silva, G.B.S. Séries Temporais de NDVI Do Sensor SPOT Vegetation e Algoritmo SAM Aplicados Ao Mapeamento de Cana-de-açúcar. *Pesqui. Agropecu. Bras.* **2012**, *47*, 1337–1345. [CrossRef]
101. Artigas, R.C.; Del Olmo, F.D. Muestreo En Transecto de Formaciones Vegetales de Fanerófitos y Caméfitos (I): Fundamentos Metodológicos. *Estud. Geogr.* **2013**, *74*, 67–88. [CrossRef]
102. Younes, N.; Joyce, K.E.; Maier, S.W. All Models of Satellite-Derived Phenology Are Wrong, but Some Are Useful: A Case Study from Northern Australia. *Int. J. Appl. Earth Obs. Geoinf.* **2021**, *97*, 102285. [CrossRef]
103. Paci, L.; Gelfand, A.E.; Beamonte, M.A.; Rodrigues, M.; Pérez-Cabello, F. Space-Time Modeling for Post-Fire Vegetation Recovery. *Stoch. Environ. Res. Risk Assess.* **2015**, *31*, 171–183. [CrossRef]
104. Cruz, Ó.; Riveiro, S.F.; García-Duro, J.; Casal, M.; Reyes, O. European Atlantic Deciduous Forests Are More Resilient to Fires than Pinus and Eucalyptus Plantations. *For. Ecol. Manag.* **2024**, *561*, 121849. [CrossRef]
105. Holling, C.S. Resilience and Stability of Ecological Systems. *Annu. Rev. Ecol. Evol. Syst.* **1973**, *4*, 1–23. [CrossRef]
106. Ruffault, J.; Curt, T.; Moron, V.; Trigo, R.M.; Mouillot, F.; Koutsias, N.; Pimont, F.; Martin-StPaul, N.; Barbero, R.; Dupuy, J.L.; et al. Increased Likelihood of Heat-Induced Large Wildfires in the Mediterranean Basin. *Sci. Rep.* **2020**, *10*, 13790. [CrossRef] [PubMed]
107. Meng, J.N.; Fang, H.; Scavia, D. Application of Ecosystem Stability and Regime Shift Theories in Ecosystem Assessment-Calculation Variable and Practical Performance. *Ecol. Indic.* **2021**, *125*, 107529. [CrossRef]
108. Selles, O.A.; Rissman, A.R. Content Analysis of Resilience in Forest Fire Science and Management. *Land Use Policy* **2020**, *94*, 104483. [CrossRef]
109. Fan, X.; Hao, X.; Hao, H.; Zhang, J.; Li, Y. Comprehensive Assessment Indicator of Ecosystem Resilience in Central Asia. *Water* **2021**, *13*, 124. [CrossRef]
110. Lloret, F.; Jaime, L.A.; Margalef-Marrase, J.; Pérez-Navarro, M.A.; Batllori, E. Short-Term Forest Resilience after Drought-Induced Die-off in Southwestern European Forests. *Sci. Total Environ.* **2022**, *806*, 150940. [CrossRef]
111. Folke, C.; Carpenter, S.R.; Walker, B.; Scheffer, M.; Chapin, T.; Rockström, J. Resilience Thinking: Integrating Resilience, Adaptability and Transformability. *Ecol. Soc.* **2010**, *15*, 20. [CrossRef]
112. Ma, J.; Zhang, C.; Li, S.; Yang, C.; Chen, C.; Yun, W. Changes in Vegetation Resistance and Resilience under Different Drought Disturbances Based on NDVI and SPEI Time Series Data in Jilin Province, China. *Remote Sens.* **2023**, *15*, 3280. [CrossRef]
113. Prodon, R.; Diaz-Delgado, R. Assessing the Postfire Resilience of a Mediterranean Forest from Satellite and Ground Data (NDVI, Vegetation Profile, Avifauna). *Écoscience* **2021**, *28*, 81–91. [CrossRef]
114. Camarero, J.J.; Guijarro, M.; Calama, R.; Valeriano, C.; Pizarro, M.; Madrigal, J. Wildfires Improve Forest Growth Resilience to Drought. *Fire* **2023**, *6*, 161. [CrossRef]
115. Lv, X.; Chen, G.; Wang, Q.; Chen, T. Exploring the Resilience of Global Vegetation Ecosystem: Nonlinearity, Driving Forces, and Management. *J. Environ. Manag.* **2025**, *377*, 124634. [CrossRef]
116. Shu, Y.; Shi, C.; Yi, B.; Zhao, P.; Guan, L.; Zhou, M. Influence of Climatic Factors on Lightning Fires in the Primeval Forest Region of the Northern Daxing'an Mountains, China. *Sustainability* **2022**, *14*, 5462. [CrossRef]

117. Blanco-Rodríguez, M.Á.; Ameztegui, A.; Gelabert, P.; Rodrigues, M.; Coll, L. Short-Term Recovery of Post-Fire Vegetation Is Primarily Limited by Drought in Mediterranean Forest Ecosystems. *Fire Ecol.* **2023**, *19*, 68. [CrossRef]
118. Chen, X.; Chen, W.; Xu, M. Remote-Sensing Monitoring of Postfire Vegetation Dynamics in the Greater Hinggan Mountain Range Based on Long Time-Series Data: Analysis of the Effects of Six Topographic and Climatic Factors. *Remote Sens.* **2022**, *14*, 2958. [CrossRef]
119. Moravec, J. Regeneration of N.W. African *Pinus halepensis* Forests Following Fire. *Vegetatio* **1990**, *87*, 29–36. [CrossRef]
120. Le Houerou, H.N. *Fire and Vegetation in the Mediterranean Basin*; Plant Production and Protection Division: Rome, Italy, 1974; pp. 237–277.
121. Pausas, J.G.; Gimeno, T.; Vallejo, R. Fire Severity and Pine Regeneration in the Eastern Iberian Peninsula. In *Forest Fire Research and Wildland Fire Safety*; Millpress: Rotterdam, The Netherlands, 2002; pp. 1–8.
122. Baeza, M.J.; Valdecantos, A.; Alloza, J.A.; Vallejo, V.R. Human Disturbance and Environmental Factors as Drivers of Long-Term Post-Fire Regeneration Patterns in Mediterranean Forests. *J. Veg. Sci.* **2007**, *18*, 243–252. [CrossRef]
123. Vicente-Serrano, S.M.; Pérez-Cabello, F.; Lasanta, T. *Pinus halepensis* Regeneration after a Wildfire in a Semiarid Environment: Assessment Using Multitemporal Landsat Images. *Int. J. Wildl. Fire* **2011**, *20*, 195–208. [CrossRef]
124. Pérez Cabello, F.; Ibarra, P. Procesos de Regen- Eración Vegetal En Comunidades Incendiadas (Prepirineo Oscense). In *Aspectos Generales Y Temáticos*; Peña Monné, J.L., Longares Aladrén, L.A., Sánchez Fabre, M., Eds.; Geografía Física de Aragón: Zaragoza, Spain, 2004.
125. Trabaud, L. Recuperación y Regeneración de Ecosistemas Mediterráneos Incendiados. *Ser. Geogr.* **1998**, *7*, 37–47.
126. Broncano, M.J.; Retana, J.; Rodrigo, A. Predicting the Recovery of *Pinus halepensis* and Quercus Ilex Forests after a Large Wildfire in Northeastern Spain. *Plant Ecol.* **2005**, *180*, 47–56. [CrossRef]
127. Kazanis, D.; Spatharis, S.; Kokkoris, G.D.; Dimitrakopoulos, P.G.; Arianoutsou, M. Drivers of *Pinus halepensis* Plant Community Structure across a Post-Fire Chronosequence. *Fire* **2024**, *7*, 331. [CrossRef]
128. Thanos, C.A.; Daskalakou, E.N.; Nikolaidou, S. Early Post-fire Regeneration of a *Pinus halepensis* Forest on Mount Párnis, Greece. *J. Veg. Sci.* **1996**, *7*, 273–280. [CrossRef]
129. Zalba, S.M.; Cuevas, Y.A.; Boó, R.M. Invasion of *Pinus halepensis* Mill. Following a Wildfire in an Argentine Grassland Nature Reserve. *J. Environ. Manag.* **2008**, *88*, 539–546. [CrossRef]
130. Elvira, N.J.; Lloret, F.; Jaime, L.; Margalef-Marrase, J.; Pérez Navarro, M.Á.; Batllori, E. Species Climatic Niche Explains Post-Fire Regeneration of Aleppo Pine (*Pinus halepensis* Mill.) under Compounded Effects of Fire and Drought in East Spain. *Sci. Total Environ.* **2021**, *798*, 149308. [CrossRef]
131. Kazanis, D.; Xanthopoulos, G.; Arianoutsou, M. Long-Term Post-Fire Evolution of Understorey Biomass in *Pinus halepensis* Mill. *For. Cent. Greece* **2006**, *234*, S175.
132. Daskalakou, E.N.; Thanos, C.A. Postfire Seedling Dynamics and Performance in *Pinus halepensis* Mill. Populations. *Acta Oecol.* **2010**, *36*, 446–453. [CrossRef]
133. Ne'eman, G. Regeneration of Natural Pine Forest—Review of Work Done after the 1989 Fire in Mount Carmel, Israel. *Int. J. Wildl. Fire* **1997**, *7*, 295–306. [CrossRef]
134. González-De Vega, S.; De las Heras, J.; Moya, D. Resilience of Mediterranean Terrestrial Ecosystems and Fire Severity in Semiarid Areas: Responses of Aleppo Pine Forests in the Short, Mid and Long Term. *Sci. Total Environ.* **2016**, *573*, 1171–1177. [CrossRef]
135. Cabanillas-Saldana, A.M. Bases Para La Gestión de Masas Naturales de *Pinus halepensis* Mill. en el Valle del Ebro. Doctoral Dissertation, Escuela Técnica Superior de Ingenieros de Montes, Universidad Politécnica de Madrid, Madrid, Spain, 2010; p. 199.
136. Gong, P.; Pu, R.; Biging, G.S.; Larrieu, M.R. Estimation of Forest Leaf Area Index Using Vegetation Indices Derived from Hyperion Hyperspectral Data. *IEEE Trans. Geosci. Remote Sens.* **2003**, *41*, 1355–1362. [CrossRef]
137. Riaño, D.; Chuvieco, E.; Ustin, S.; Zomer, R.; Dennison, P.; Roberts, D.; Salas, J. Assessment of Vegetation Regeneration after Fire through Multitemporal Analysis of AVIRIS Images in the Santa Monica Mountains. *Remote Sens. Environ.* **2002**, *79*, 60–71. [CrossRef]
138. Pickell, P.D.; Hermosilla, T.; Frazier, R.J.; Coops, N.C.; Wulder, M.A. Forest Recovery Trends Derived from Landsat Time Series for North American Boreal Forests. *Int. J. Remote Sens.* **2016**, *37*, 138–149. [CrossRef]
139. Kurbanov, E.; Tarasova, L.; Yakhyayev, A.; Vorobev, O.; Gozalov, S.; Lezhnin, S.; Wang, J.; Sha, J.; Dergunov, D.; Yastrebova, A. Detecting Trends in Post-Fire Forest Recovery in Middle Volga from 2000 to 2023. *Forests* **2024**, *15*, 1919. [CrossRef]
140. Saracino, A.; Leone, V.; Trabaud, L.; Prodon, R. Natural Regeneration 2 and 4 Years after Fire of *Pinus halepensis* Miller in Dunal Environment. In *Fire in Mediterranean Ecosystems*; E. Guyot SA: Brussels, Belgium, 1993; pp. 141–151. [CrossRef]
141. Herranz, J.M.; Martínez-Sánchez, J.J.; Marín, A.; Ferrandis, P. Postfire Regeneration of *Pinus halepensis* Miller in a Semi-Arid Area in Albacete Province (Southeastern Spain). *Ecoscience* **1997**, *4*, 86–90. [CrossRef]
142. José Martínez-Sánchez, J.; Ferrandis, P.; De Las Heras, J.; María Herranz, J. Effect of Burnt Wood Removal on the Natural Regeneration of *Pinus halepensis* after Fire in a Pine Forest in Tus Valley (SE Spain). *For. Ecol. Manag.* **1999**, *123*, 1–10. [CrossRef]

143. Arianoutsou, M.; Ne'eman, G. Post-Fire Regeneration of Natural *Pinus halepensis* Forests in the East Mediterranean Basin. In *Ecology, Biogeography and Management of Pinus halepensis and P. brutia Forest Ecosystems in the Mediterranean Basin*; Backhuys Publishers: Leiden, The Netherlands, 2000; pp. 269–290.
144. Pausas, J.G.; Ribeiro, E.; Vallejo, R. Post-Fire Regeneration Variability of *Pinus halepensis* in the Eastern Iberian Peninsula. *For. Ecol. Manag.* **2004**, *203*, 251–259. [CrossRef]
145. Moya, D.; González-De Vega, S.; Lozano, E.; García-Orenes, F.; Mataix-Solera, J.; Lucas-Borja, M.E.; de las Heras, J. The Burn Severity and Plant Recovery Relationship Affect the Biological and Chemical Soil Properties of *Pinus halepensis* Mill. Stands in the Short and Mid-Terms after Wildfire. *J. Environ. Manag.* **2019**, *235*, 250–256. [CrossRef]